

**Review**

# Liquid electrolyte: The nexus of practical lithium metal batteries

Hansen Wang,<sup>1,5</sup> Zhiao Yu,<sup>2,3,5</sup> Xian Kong,<sup>2</sup> Sang Cheol Kim,<sup>1</sup> David T. Boyle,<sup>1,3</sup> Jian Qin,<sup>2</sup> Zhenan Bao,<sup>2,\*</sup> and Yi Cui<sup>1,4,\*</sup>

**SUMMARY**

The specific energy of commercial lithium (Li)-ion batteries is reaching the theoretical limit. Future consumer electronics and electric vehicle markets call for the development of high energy density Li metal batteries, which have been plagued by poor cyclability. Electrolyte engineering can afford a promising approach to address the issues associated with Li metal batteries and has recently resulted in much improved cycle life under practical conditions. However, gaps still exist between the performance of current Li metal batteries and those required for commercial applications. Further improvements will require systematic analysis of existing electrolyte design methodologies. In this review, we first summarize recent approaches of advanced electrolytes for Li metal batteries paired with high-voltage cathodes. We then extract common features among these advanced electrolytes and finally discuss the future rational design directions and strategies.

**INTRODUCTION**

Lithium (Li)-ion batteries (LIBs) have dramatically changed our society with their broad applications in portable electronics and electric vehicles. However, their specific energies are reaching the theoretical limit with their graphite-based anodes.<sup>1</sup> Substantial efforts in both industry and academia have been made to revive Li metal batteries (LMBs), a technology explored and commercialized before LIBs but was prevented from widespread adoption due to its safety concerns and limited cyclability.<sup>2</sup> With the highest specific capacity (3,860 mAh/g) and the lowest reduction potential (−3.04 V versus standard hydrogen electrode [SHE]), Li metal anodes (LMAs) can potentially enable batteries with the highest specific energy.<sup>3,4</sup> However, these batteries usually have shorter cycle lives and potential safety hazards due to the high reactivity and volume fluctuations of LMAs.<sup>5,6</sup> Multiple strategies have been explored to address these issues, including 3-dimensional “host” structures,<sup>7–13</sup> artificial coatings,<sup>14–22</sup> and electrolyte engineering.<sup>6,23–27</sup> However, further developments are still needed for LMBs to meet the requirements of practical applications.

Ether-based electrolytes were predominantly used in the early decades of LMA research due to their decent reductive stability.<sup>28–30</sup> However, with the discovery of high-voltage cathodes, such as layered transition metal oxides  $\text{LiNi}_x\text{Mn}_y\text{Co}_z\text{O}_2$  (NMC),<sup>31</sup> common ether solvents fell short in Li metal full cells due to their poor oxidative stability.<sup>32</sup> It is noteworthy that we herein describe >4.2 V as high voltage, because this upper voltage cut-off is commonly used in both academia and industry, covering NMC cathode family,  $\text{LiCoO}_2$  (LCO),  $\text{LiMn}_2\text{O}_4$  (LMO),  $\text{LiNi}_{0.5}\text{Mn}_{1.5}\text{O}_4$  (LNMO),  $\text{LiCoPO}_4$  (LCP), Li-rich cathodes, etc. With the successful commercialization

**Context & scale**

Lithium (Li)-ion batteries have significantly advanced our society with their broad applications in portable electronic devices, electric vehicles, and grid storage.

However, the energy density of Li-ion battery systems is reaching the theoretical limit, therefore, raising the urgent need for further improvement in the energy density of next-generation battery systems.

Li metal batteries have been acknowledged as a promising alternative choice, yet they have been plagued by poor cyclability, which originates from significant electrode volume change, dendritic growth, and uncontrollable side reactions during Li metal cycling.

During the past decades, cycling efficiency of Li metal anodes have been significantly improved from ~80% to ~99.5% through gradual exploration and optimization of electrolyte formulations. Although still insufficient for commercial applications, such progress demonstrates the feasibility of further electrolyte engineering in enabling Li metal batteries. In this review, we systematically summarize past designs of Li metal battery electrolytes, conclude the key features of advanced electrolyte formulations, and then propose detailed design principles and methodologies that are critical for future developments of advanced Li metal battery electrolytes.



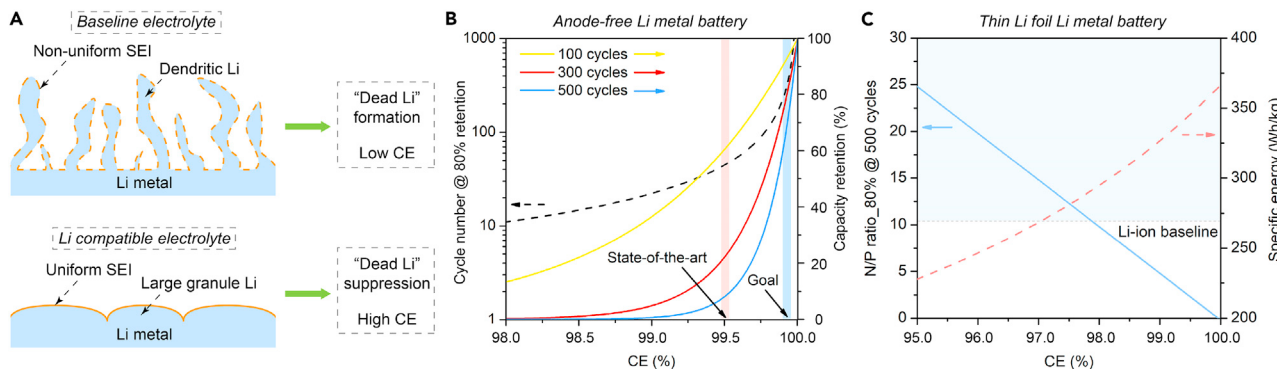


**Figure 1. Opportunities and challenges of electrolyte engineering for LMBs**

- (A) Schematic comparing Li metal cycling in baseline electrolyte and in recently developed high-performance electrolytes.  
 (B) Theoretical plot of cycle number after reaching 80% capacity retention and capacity retention after 100, 300 and 500 cycles as a function of CE for anode-free LMBs.  
 (C) Theoretical plot of the N/P ratio required to achieve 80% capacity retention after 500 cycles and the corresponding full-cell specific energy as a function of CE for thin Li foil LMBs.

of LIBs, carbonate-based, standard-concentration electrolytes were also investigated for the use in LMBs.<sup>7,9,33</sup> Although these electrolytes were compatible with LIBs using high-voltage cathodes, they have been found unstable for Li metal cycling. They form non-uniform solid-electrolyte interphase (SEI), leading to dendritic growth, extensive “dead Li” formation,<sup>2</sup> low Coulombic efficiency (CE), and poor cycle life (Figure 1A). In the last decade, researchers started to discover new strategies, including enhancing electrolyte concentrations,<sup>34</sup> designing new fluorinated solvent molecules,<sup>35</sup> tuning electrolyte additives,<sup>36</sup> etc., that dramatically improved the electrolyte stability for use with both LMAs and high-voltage cathodes. These new electrolytes enabled more stable and uniform SEIs, larger granules of deposited Li, suppressed “dead Li” formation, and the subsequent high CEs<sup>37,38</sup> (Figure 1A). Recently, the cycle life of LMBs has been raised to an unprecedented level simply by tuning the electrolyte formulation. Therefore, liquid electrolyte engineering is a promising approach to enabling practical LMBs.<sup>6</sup>

Despite these successes, a considerable gap still exists between current LMB performance and practical requirements when taking specific energy and cycle life as the primary figure of merit.<sup>39</sup> For example, for an anode-free LMB to achieve 80% capacity retention after 500 cycles, a Li metal cycling CE of >99.96% is needed (Figure 1B). With the intrinsically impeded lithiation at the end of the 1<sup>st</sup> discharge of NMC cathodes,<sup>40,41</sup> ~10%–15% of Li remains on the anode side serving as an excess Li reservoir after the first cycle, but still a CE of >99.93% is needed. Currently, state-of-the-art LMB electrolytes only achieved CEs around ~99.5%.<sup>35,42</sup> LMBs with thin Li foil anodes can ease the requirements on CE, but the additional Li reservoir can lower the specific energy of the battery. To simultaneously achieve 350 Wh/kg and 80% capacity retention after 500 cycles, a CE of >99.62% is needed with a N/P ratio (the ratio of negative electrode capacity to positive electrode capacity) of 1.7 (Figure 1C). Although some electrolytes are approaching this CE value for LMAs, realizing the corresponding full cell with lean electrolyte and limited Li excess is still challenging<sup>43</sup> because of failure mechanisms other than the loss of active Li, such as electrolyte dry-out or impedance build-up.<sup>44</sup> Furthermore, the use of thin Li foil increases the cost and complexity of large-scale cell production,<sup>39</sup> adding concerns to its commercialization.<sup>45</sup> In summary, innovations on LMB electrolytes are needed to further improve the CE of LMAs and enable the successful development of LMBs. To guide

<sup>1</sup>Department of Materials Science and Engineering, Stanford University, Stanford, CA, USA

<sup>2</sup>Department of Chemical Engineering, Stanford University, Stanford, CA, USA

<sup>3</sup>Department of Chemistry, Stanford University, Stanford, CA, USA

<sup>4</sup>Stanford Institute for Materials and Energy Sciences, SLAC National Accelerator Laboratory, Menlo Park, CA, USA

<sup>5</sup>These authors contributed equally

\*Correspondence: zbao@stanford.edu (Z.B.), yicui@stanford.edu (Y.C.)

<https://doi.org/10.1016/j.joule.2021.12.018>

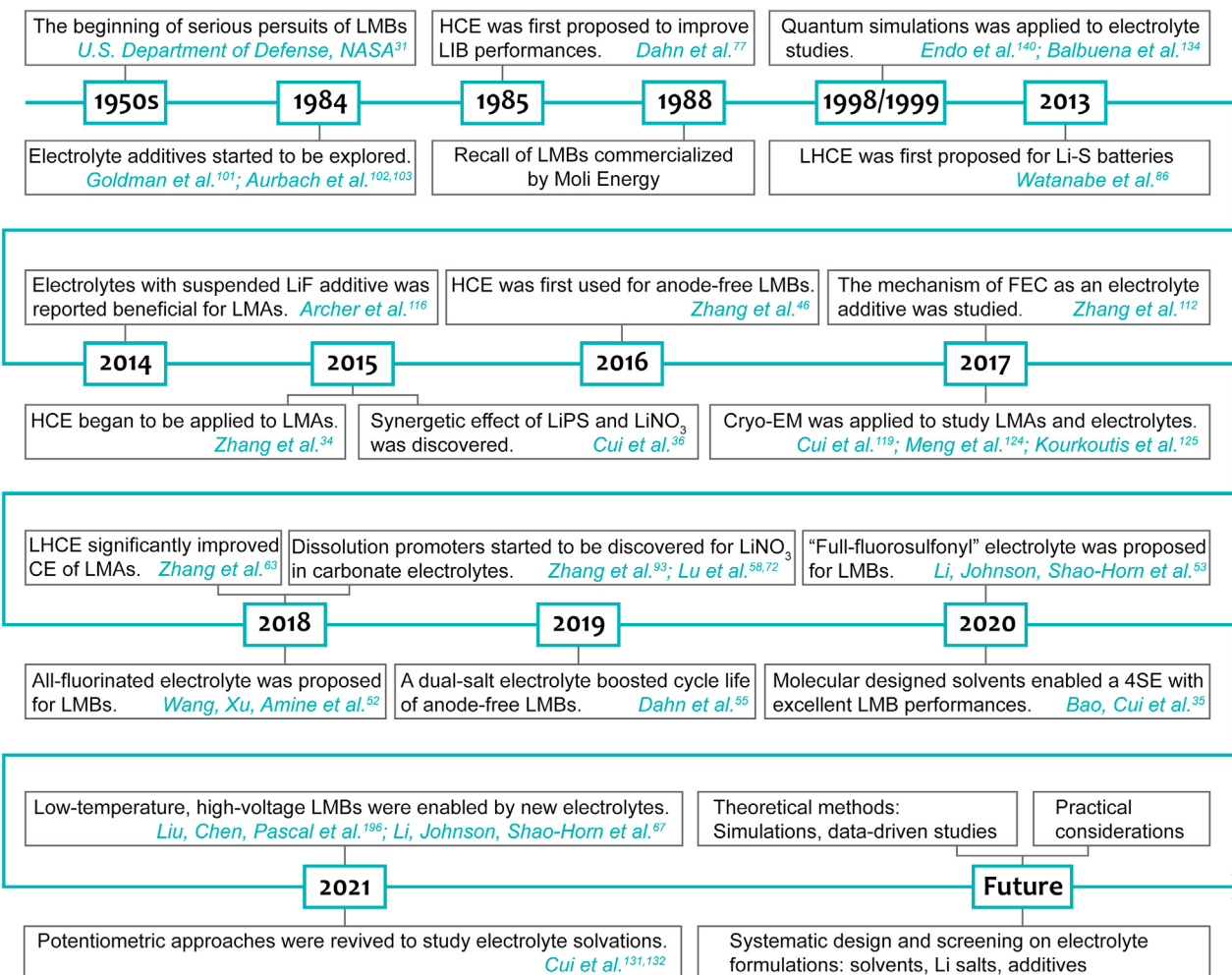


**Figure 2. A roadmap of electrolyte developments for LMBs**

further design and optimization of electrolyte formulations, systematic reflection of recent electrolyte engineering research is necessary.

In this review (Figure 2; Tables 1 and 2; Appendix 1), we first summarize recent electrolyte design strategies for LMBs with high-voltage cathodes. Then, we identify several shared features and properties of these new electrolyte formulations that are potentially the key directions to enable long cycle life of LMBs. Finally, we propose several strategies to further optimize the electrolyte formulations for practical LMBs.

## RECENT PROGRESS IN HIGH-PERFORMANCE ELECTROLYTES FOR LMBs

### High concentration electrolytes (HCEs)

The strategy of enhancing electrolyte concentrations to improve battery performance originated from LIB research.<sup>75,76</sup> In 1985, McKinnon and Dahn first discovered that saturated LiAsF<sub>6</sub> in propylene carbonate (PC) could prevent the co-intercalation of PC into ZrS<sub>2</sub> electrodes.<sup>77</sup> Jeong et al. also reported in 2003<sup>78</sup> and 2008<sup>79</sup> that concentrated LiClO<sub>4</sub>, LiPF<sub>6</sub>, and LiN(SO<sub>2</sub>C<sub>2</sub>F<sub>5</sub>)<sub>2</sub> (LiBETI) salts in PC (>2.5 M) could effectively suppress the co-intercalation of PC into graphite anodes. In 2010<sup>80</sup> and 2014,<sup>81</sup> Yamada et al. further

**Table 1.** Recently reported electrolytes with excellent anode-free battery performances

Electrolyte type	Electrolyte formulation	Electrolyte amount	Cell condition	Cycling condition & capacity retention
HCEs	4 M LiFSI/DME <sup>46</sup>	~44 g/Ah	1.71 mAh/cm <sup>2</sup> Cu  LFP coin cell	3.8 V, ~C/8 cycling, 60% @ 50 cycles
	7 M LiFSI/FEC <sup>47</sup>	not mentioned	1.83 mAh/cm <sup>2</sup> Cu  LNMO coin cell	5 V, 54% @ 50 cycles
	3 M LiFSI/DME-DOL <sup>48</sup>	~37 mL/Ah	1.6 mAh/cm <sup>2</sup> Cu  LFP coin cell	3.8 V, 64% @ 50 cycles
	2 M LiPF <sub>6</sub> /EC-DEC-FEC <sup>49</sup>	not mentioned	~1.6 mAh/cm <sup>2</sup> Cu  NMC111 coin cell	4.3 V, ~C/8 cycling, 40% @ 50 cycles
	2 M LiPF <sub>6</sub> /THF-MTHF <sup>43</sup>	not mentioned	2.3 mAh/cm <sup>2</sup> Cu  LFP coin cell	3.5 V, ~65% @ 100 cycles
LHCEs	1LiFSI-1.2DME-3TTE <sup>50</sup>	3 g/Ah	~4.2 mAh/cm <sup>2</sup> Cu  NMC811 coin cell	4.4 V, C/3 cycling, 77% @ 70 cycles
4SEs and derived	1 M LiFSI/FDMB <sup>35</sup>	~2 g/Ah	~200 mAh Cu  NMC532 pouch cell	4.2 V, 100% DOD, C/5 D/3, 80% @ 100 cycles
	1 M LiFSI/DME-FDMH <sup>51</sup>	~2.1 mL/Ah	~200 mAh Cu  NMC811 pouch cell	4.2 V, 100% DOD, C/5 D/4, 75% @ 120 cycles
FFE <sub>s</sub>	1 M LiPF <sub>6</sub> /FEC-FEMC-D2 <sup>52</sup>	~47 g/Ah	~2.0 mAh/cm <sup>2</sup> Cu  NMC811 coin cell	4.4 V, ~C/4 cycling, 50% @ 30 cycles
	1 M LiFSI/FSA <sup>53</sup>	~25 mL/Ah	1.6 mAh/cm <sup>2</sup> Cu  NMC622 coin cell	4.3 V, C/10 D/3, 50.8% @ 45 cycles
Multi-salt electrolytes	1 M LiTFSI + 2 M LiFSI + 3 wt % LiNO <sub>3</sub> / DME-DOL <sup>54</sup>	not mentioned	0.85 mAh/cm <sup>2</sup> Cu  LFP coin cell	3.8 V, C/4 cycling, 39% @ 100 cycles
	1 M LiDFOB + 0.2 M LiBF <sub>4</sub> /FEC-DEC <sup>55</sup>	~2 g/Ah	~245 mAh Cu  NMC532 pouch cell	3.6–4.5 V, C/5 D/2, 40°C, 80% @ 90 cycles
	1.8 M LiDFOB + 0.4 M LiBF <sub>4</sub> /FEC-DEC <sup>56</sup>	~2 g/Ah	~210 mAh Cu  NMC532 pouch cell	3.6–4.5 V, C/5 D/2, 40°C hot formed, 80% @ 195 cycles (high pressure)
	2 M LiDFOB + 1.4 M LiBF <sub>4</sub> /FEC-DEC <sup>39</sup>	~2.2 mL/Ah	~230 mAh Cu  NMC532 pouch cell	3.6–4.5 V, C/5 D/2, 40°C hot formed, 80% @ 200 cycles (high pressure)
Electrolytes with novel additives	1 M LiPF <sub>6</sub> /FEC-TFFC <sup>57</sup>	3 g/Ah	~230 mAh Cu  532 pouch cell	3.6–4.5 V, C/5 D/2, 40°C, 80% @ 40 cycles
	1 M LiPF <sub>6</sub> /EC-DEC with 10 mM In(OTf) <sub>3</sub> and 0.5 M LiNO <sub>3</sub> <sup>58</sup>	8.37g/Ah	4.3 mAh/cm <sup>2</sup> Cu  NMC811 coin cell	3–4.3 V, 0.1C 0.3D, 50% @ 80 cycles
	1 M LiTFSI + 1.5 M LiFSI /G3-HFE <sup>59</sup>	2.5 g/Ah	~4.85 mAh/cm <sup>2</sup> , 2.46 Ah Cu  NMC811+Li <sub>2</sub> O pouch cell	2.8–4.4 V, 100% DOD, 0.375C 0.5D, 80% @ 300 cycles

applied this strategy to other solvents, such as dimethyl sulfoxide (DMSO) and acetonitrile (AN), with 3.2–4 M LiN(SO<sub>2</sub>CF<sub>3</sub>)<sub>2</sub> (LiTFSI) as the salt. By combining density functional theory calculation with molecular dynamics simulations (DFT-MD), they found that **HCEs effectively reduced the number of solvent molecules coordinated with Li-ions**. This not only contributed to the suppression of co-intercalation but also significantly improved the electrolyte reductive stability. In 2015, Suo et al. applied this strategy to water-based electrolytes, which enabled the first aqueous LIB chemistry.<sup>82</sup>

Jeong et al. first explored the performance of HCEs for Li metal cycling in 2008.<sup>83</sup> They reported an improved CE for Li metal with high concentrations of 3.27 M LiBETI in PC, but the choices of Li salt and solvent were not optimized, and the CE was still below 85%. A significant milestone on HCEs was published in 2015, where Qian et al. reported that 4 M LiN(SO<sub>2</sub>F)<sub>2</sub> (LiFSI) in 1,2-dimethoxyethane (DME)<sup>34</sup> enabled a high Li cycling CE: 99.1% under 0.2 mA/cm<sup>2</sup> and 98.4% under 4 mA/cm<sup>2</sup>. In this work, LiFSI was chosen as the salt due to its high ionic conductivity and solubility, whereas DME was selected as the solvent due to its excellent stability toward LMAs. The high electrolyte concentration significantly reduced the amount of uncoordinated DME and enhanced the coordination of FSI<sup>-</sup> anions to Li-ions (Figure 3A). Such solvation environments improved the electrolyte's reductive<sup>34</sup> and oxidative<sup>46,84</sup> stability and allowed them to form inorganic-rich SEIs with lower ionic resistances. The electrolyte not only deposited Li in large granules with excellent cycling efficiencies (Figure 3B) but was also compatible with high-voltage cathodes, such as NMC. The stable cycling of Li with the tuning of the electrolyte formulation has inspired a series of works optimizing HCEs for LMBs.

In 2018, Fan et al. reported HCEs with 10 M LiFSI in dimethyl carbonate (DMC) or ethylene carbonate (EC)-DMC mixture, achieving a high Li cycling CE of 99.3%.<sup>60</sup> Li||NMC622 full cells were found to stably cycle at 4.6 V with 86% capacity retention after

**Table 2.** Recently reported electrolytes with good performances for LMBs with excess Li

Electrolyte type	Electrolyte formulation	Electrolyte amount	Cell condition	Cycling condition & capacity retention
HCEs	4 M LiFSI/DME <sup>46</sup>	~37 mL/Ah	Li  NMC111 (1.5 mAh/cm <sup>2</sup> ), N/P = 60	4.3 V, C/3 1D, 92% @ 500 cycles
	10 M LiFSI/EC-DMC <sup>60</sup>	not mentioned	Li  NMC622 (13 mg/cm <sup>2</sup> )	4.6 V, 86% @ 100 cycles
	7 M LiFSI/FEC <sup>47</sup>	not mentioned	Li  LNMO (1.83 mAh/cm <sup>2</sup> ), N/P = 1.4	5 V, ~70% @ 140 cycles
	1:2.5 LiFSI/SL <sup>61</sup>	~30 mL/Ah	Li  LFP (1.76 mAh/cm <sup>2</sup> ), N/P=2.34	3.8 V, 0.5C cycling, 92.7% @ 140 cycles
	4 M LiFSI/DEE <sup>62</sup>	8 g/Ah	Li  NMC811 (4.8 mAh/cm <sup>2</sup> ), N/P = 2	4.4 V, 0.2C 0.3D, 80% @ 182–200 cycles
LHCEs	1.2 M LiFSI/DMC-BTTF <sup>63</sup>	~79 mL/Ah	Li  NMC111 (2 mAh/cm <sup>2</sup> ), N/P = 45	4.3 V, 0.5C 2D, 80% @ 700 cycles
	1.2 M LiFSI/TEP-BTTF <sup>64</sup>	~50 mL/Ah	Li  NMC622 (1.6 mAh/cm <sup>2</sup> ), N/P = 56.25	4.4 V, C/3 1D, ~97% @ 600 cycles
	1.2 M LiFSI + 0.15 M LiDFOB/EC-EMC-BTTF <sup>65</sup>	~6.6 mL/Ah	Li  NMC111 (3 mAh/cm <sup>2</sup> ), N/P = 3.33	4.3 V, C/3 cycling, ~80% @ ~85 cycles
	1LiFSI-3TMS-3TTE <sup>66</sup>	~39 mL/Ah	Li  NMC (1.5 mAh/cm <sup>2</sup> ), N/P = 6.67	4.3 V, C/3 cycling, ~80% @ 300 cycles
	1LiFSI-1.2DME-3TTE <sup>50</sup>	3 g/Ah	Li  NMC811 (4.2 mAh/cm <sup>2</sup> ), N/P = 2.4	4.4 V, C/3 cycling, 80% @ 155 cycles
4SEs and derived	1 M LiFSI/DME/TFFO <sup>42</sup>	50 g/Ah	Li  NMC811 (1.5 mAh/cm <sup>2</sup> ), N/P = 6.7	4.4 V, C/3 cycling, 80% @ 300 cycles
	1 M LiFSI/FDMM <sup>35</sup>	~30 g/Ah	Li  NMC532 (1.6 mAh/cm <sup>2</sup> ), N/P = 6	4.2 V, C/3 cycling, 90% @ 400 cycles
	1 M LiFSI/FDMM <sup>35</sup>	~6 g/Ah	Li  NMC532 (1.6 mAh/cm <sup>2</sup> ), N/P = 2.5	4.2 V, C/3 cycling, 100% @ 210 cycles
	1 M LiFSI/DME-FDMH <sup>51</sup>	~8 mL/Ah	Li  NMC532 (2.5 mAh/cm <sup>2</sup> ), N/P = 1.6	4.2 V, C/3 cycling, 84% @ 250 cycles
	1 M LiFSI/DME-FDMH <sup>51</sup>	~10 mL/Ah	Li  NMC811 (2 mAh/cm <sup>2</sup> ), N/P = 2	4.4 V, C/2 cycling, 76% @ 250 cycles
FFEes	1 M LiPF <sub>6</sub> /FEC-FEMC-D2 <sup>52</sup>	~50 g/Ah	Li  NMC811 (2 mAh/cm <sup>2</sup> ), N/P = 1	4.4 V, ~C/2 cycling, 95% @ 120 cycles
	1 M LiFSI/FSA <sup>53</sup>	~25 mL/Ah	Li  NMC622 (1.6 mAh/cm <sup>2</sup> ), N/P = 7.6	4.3 V, 89% @ 200 cycles
	1 M LiFSI/DMTMSA <sup>67</sup>	2.62 g/Ah	Li  NMC811 (4.86 mAh/cm <sup>2</sup> ), N/P = 0.39	4.7 V, 0.15C 0.5D, 88% @ 90 cycles
Multi-salt electrolytes	2 M LiTFSI + 2 M LiDFOB/DME <sup>68</sup>	~40 mL/Ah	Li  NMC111 (1.7 mAh/cm <sup>2</sup> ), N/P = 30	4.3 V, C/3 1D, 79% @ 500 cycles
	1 M LiTFSI + 2 M LiFSI + 3 wt % LiNO <sub>3</sub> /DME-DOL <sup>54</sup>	Not mentioned	Li  LFP (0.85 mAh/cm <sup>2</sup> ), N/P = 0.44	3.8 V, C/4 cycling, 83% @ 100 cycles
Electrolytes with novel additives	0.5 M LiPF <sub>6</sub> /EC-DEC with LiNO <sub>3</sub> <sup>69</sup>	~80 mL/Ah	Li  NMC (8 mg/cm <sup>2</sup> ), N/P = 8.4	4.3 V, ~1C cycling, ~80% @ 250 cycles
	1.0 M LiPF <sub>6</sub> /FEC-DMC-DME with 1.1 wt % LiNO <sub>3</sub> <sup>70</sup>	Not mentioned	Li  LFP (2 mAh/cm <sup>2</sup> ), N/P = 5	4 V, 0.2C cycling, ~85% @ 120 cycles
	2.3 M LiFSI/DME with 20 mM of LiNO <sub>3</sub> and 20 mM of CuF <sub>2</sub> <sup>71</sup>	4 mL/Ah	Li  LFP (2 mAh/cm <sup>2</sup> ), N/P = 5	4 V, 0.2C cycling, 100% @ 80 cycles
	1 M LiPF <sub>6</sub> /EC-DEC with 10 mM In(OTf) <sub>3</sub> and 0.5 M LiNO <sub>3</sub> <sup>58</sup>	8.37 g/Ah	Li  NMC811 (4.3 mAh/cm <sup>2</sup> ), N/P = 2.09	4.3 V, 0.3C 0.5D, 80% @ 160 cycles
	1 M LiPF <sub>6</sub> /FEC-EMC with 3 wt % LiNO <sub>3</sub> and 1 wt % TPFPB <sup>72</sup>	3.4 g/Ah	Li  NMC811 (3.4 mAh/cm <sup>2</sup> ), N/P = 2.68	4.4 V, 0.1C 0.3D, 80% @ 140 cycles
	0.8 M LiPF <sub>6</sub> /FEC-DMC with 5 wt % 4 M LiNO <sub>3</sub> /DMSO <sup>73</sup>	~7.9 mL/Ah	Li  NMC811 (2.5 mAh/cm <sup>2</sup> ), N/P = 4	4.4 V, 0.5C cycling, 75% @ 200 cycles
	0.8 M LiTFSI + 0.2 M LiDFOB + 0.05 M LiPF <sub>6</sub> /EMC-FEC (v/v, 3:1) with 1 wt % P <sub>2</sub> S <sub>5</sub> -saturated CS <sub>2</sub> <sup>74</sup>	4 mL/Ah	Li  NCMA (4 mAh/cm <sup>2</sup> ), N/P = 5	4.3 V, 0.2C 0.5D, ~80% @ 130 cycles

100 cycles. Suo et al. reported 7 M LiFSI in fluoroethylene carbonate (FEC) electrolyte had an excellent CE of 99.6%,<sup>47</sup> although it needs ~300 cycles for the CE to gradually increase and stabilize. Li||LNMO cells with limited excess Li cycled at 5 V with ~70% capacity retention after 140 cycles. Zeng et al. reported that LiFSI in triethyl phosphate (TEP) with a molar ratio of 1:2 had a CE for Li metal over 99%,<sup>85</sup> but the performance of Li metal full cells was not demonstrated. In 2019, Maeyoshi et al. reported 1:2.5 (molar ratio) LiFSI in tetramethylene sulfone (TMS, also known as sulfolane, SL) had a CE of 98%. Li||LFP cells lasted 140 cycles with 92.7% capacity retention.<sup>61</sup> Besides HCEs, there were also several reports using moderately concentrated (2–3 M) electrolyte formulations. In 2019, Hwang and co-workers reported 3 M LiFSI/DME-DOL<sup>48</sup> and 2 M LiPF<sub>6</sub>/EC-DEC-FEC<sup>49</sup> with enhanced anode-free battery performance. In 2020, Wang and co-workers<sup>43</sup> proposed a 2 M LiPF<sub>6</sub> in tetrahydrofuran (THF)-2-methyl tetrahydrofuran (MTHF) mixture, achieving record high Li metal CE of 99.83% on a bismuth (Bi)-graphite (Gr) composite substrate. This high CE was attributed to a LiF/organic bilayer SEI with a

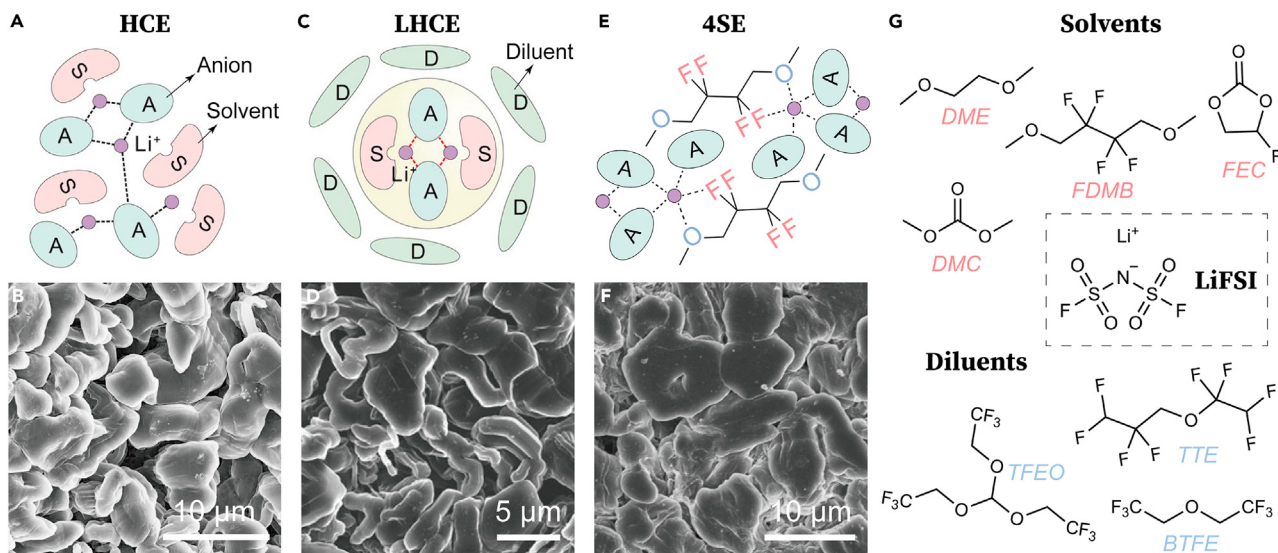


**Figure 3. HCEs, LHCEs, and 4SEs**

(A) Schematic of the solvation environment in an HCE.

(B) Li metal deposition morphology in 4 M LiFSI/DME. Reproduced with permission.<sup>34</sup> Copyright 2015, Nature Publishing Group.

(C) Schematic of the solvation environment in an LHCE.

(D) Li deposition morphology in 1.2 M LiFSI/DMC-BTFE. Reproduced with permission.<sup>63</sup> Copyright 2018, Wiley.

(E) Schematic of the solvation environment in 1 M LiFSI/FDME.

(F) Li deposition morphology in 1 M LiFSI/FDME. Reproduced with permission.<sup>35</sup> Copyright 2020, Nature Publishing Group.

(G) Solvents, diluents, and Li salt (LiFSI) commonly used in these electrolytes.

nearly pure LiF inner layer directly contacting metallic Li to promote uniform deposition.

The Bi-Gr||LFP cell maintained ~65% capacity after 100 cycles, indicating a full-cell CE of ~99.6%.

HCEs brought LMB a step closer to practical applications. HCEs for LMBs with limited or zero (anode-free) excess Li started to become cyclable. However, HCEs have several drawbacks. First, HCEs usually have reduced ionic conductivity compared with standard-concentration (1M) electrolytes. For example, by increasing the concentration of LiFSI in DME from 1 to 4 M, the ionic conductivity is reduced by a factor of three.<sup>34</sup> Second, electrolyte viscosity inevitably increases under high concentrations. Therefore, HCEs require specially designed separators<sup>75</sup> and sometimes have poor wettability to the porous cathodes.<sup>6</sup> These drawbacks could possibly lead to reduced full-cell rate capability.<sup>47</sup> Furthermore, HCEs can increase the electrolyte cost by more than 400%<sup>6</sup> due to the high content of expensive Li salts.

### Localized high concentration electrolytes (LHCEs)

To address the drawbacks of HCEs, the most straightforward approach is to dilute HCEs to standard concentrations with another solvent. Although it is nontrivial to choose the added solvent since it should not disrupt the Li-ion solvation environments in HCEs, several recent works have identified a few candidates. In 2013, Dokko et al. reported that high concentration LiTFSI in triglyme (G3)/tetraglyme (G4) diluted with a hydrofluoroether 1,1,2,2-tetrafluoroethyl-2,2,3,3-tetrafluoropropyl ether (TTE) improved the cyclability of Li-sulfur (S) batteries due to the suppression of Li polysulfide dissolution.<sup>86</sup> The addition of TTE effectively reduced the electrolyte viscosity and enhanced its ionic conductivity without disrupting the solvation structure between glyme and LiTFSI. In 2015, Watanabe and co-workers reported a similar formulation with an optimized solvent ratio giving good performance of both LIBs and Li-S batteries.<sup>87</sup> In 2016, they

systematically compared a series of solvents to dilute HCEs, with the selection of toluene and TTE as the best candidates.<sup>88</sup> In 2017, Doi et al. reported a highly concentrated LiBF<sub>4</sub> in PC diluted by TTE, enabling high reversibility of LNMO cathodes.<sup>89</sup> However, none of these works explicitly demonstrated the impact of diluted HCEs on LMA cycling.

In 2018, based on their previous works on HCEs, Chen and co-workers reported a Li metal CE of 99.3% in 5.5 M LiFSI/DMC diluted with bis(2,2,2-trifluoroethyl) ether (BTFE).<sup>63</sup> Through MD simulation and Raman spectroscopy, they showed that BTFE did not participate in the direct solvation of Li-ions, whose local environment, thus, resembled those in the HCE case (Figure 3C). Therefore, they named this electrolyte a LHCE and BTFE a diluent (Figure 3G). This LHCE electrolyte enabled uniform Li deposition morphology (Figure 3D) and excellent stability toward high-voltage cathodes with a much lower equivalent concentration (1.2 M) compared with HCEs to reduce viscosity and cost. In particular, a Li||NMC111 full cell maintains 80% capacity retention after 700 cycles. This work suggests that the diluents need to be highly stable, highly miscible with co-solvents, and weakly interacting with Li-ions. Following this work, a series of LHCEs were reported, including 1.2 M LiFSI in TEP-BTFE with good fire retardency,<sup>64</sup> 1.28 M LiFSI in FEC-methyl (2,2,2-trifluoroethyl) carbonate (FEMC)-tetrafluoro-1-(2,2,2-trifluoroethoxy)ethane (D2) and 0.7 M LiBETI in FEC-diethyl carbonate (DEC)-methoxyperfluorobutane (M3) with good extreme temperature performance,<sup>90</sup> 1.2 M LiFSI with 0.15 M LiBF<sub>2</sub>(C<sub>2</sub>O<sub>4</sub>) (LiDFOB) in EC-ethyl methyl carbonate (EMC)-BTFE,<sup>65</sup> LiFSI in TMS-TTE,<sup>66</sup> LiFSI in DME-TTE,<sup>50</sup> and 1M LiFSI in DME/tris(2,2,2-trifluoroethyl)orthoformate (TFEO).<sup>42</sup> Among them, the 1LiFSI-1.2DME-3TTE (molar ratio)<sup>50</sup> achieved the best LMB cycling performance, with 99.3% CE for 300 cycles and uniform Li deposition. A Li||NMC811 (4.2 mAh/cm<sup>2</sup>) coin cell with limited excess Li (N/P ratio = 2.4) was able to maintain 80% capacity after 155 cycles under lean electrolyte condition (3 g/Ah). Even when the excess Li was replaced by bare Cu foil, 77% of capacity was still retained after 70 cycles. This was a real advance in electrolyte design because LMBs became cyclable under realistic conditions that include high cathode loadings, limited or zero excess Li, and lean electrolyte amounts.<sup>44</sup> Although the cycle life still fell short, the LHCE strategy proved to be beneficial for LMBs, and further optimizations of salt and solvents could bring further gains in performance.

### Single-salt-single-solvent electrolytes (4SEs)

In LHCEs, one good solvent is used to solvate Li-ions, whereas the other poor solvent dilutes the concentration without compromising electrolyte stability. To simplify the electrolyte composition and conduct an in-depth study on structure-performance relationships, Yu and co-workers designed a new single-salt-single-solvent, standard-concentration electrolyte (4SE), which was enabled by a rationally designed solvent molecule that could simultaneously possess high stability and Li-ion solvability.<sup>35</sup> The new solvent is a fluorinated analog of DME, where the alkyl chain was first prolonged and then decorated with –F groups, resulting in the fluorinated 1,4-dimethoxylbutane (FDMB). The –F groups were selectively functionalized on the two carbon atoms at the center, maintaining their distances to –O– groups so that FDDB could dissolve Li salts. As a result, Li-ions coordinated with O and F simultaneously to form a five-atom ring structure (Figure 3E), which gave the electrolyte a unique brownish color. With LiFSI as the salt, the 1 M LiFSI/FDDB electrolyte achieved homogeneous Li deposition (Figure 3F) and an excellent CE of 99.5%. In Cu||Li half cells, the CE reached 99% within 5 cycles, in contrast to tens or hundreds of cycles for HCEs and LHCEs. This was made possible by eliminating any unstable solvents, such as DME and DMC, in the electrolyte. Meanwhile, 1 M LiFSI/FDDB showed a high oxidative stability of ~6 V. As a result, a Li||NMC532 cell (N/P =

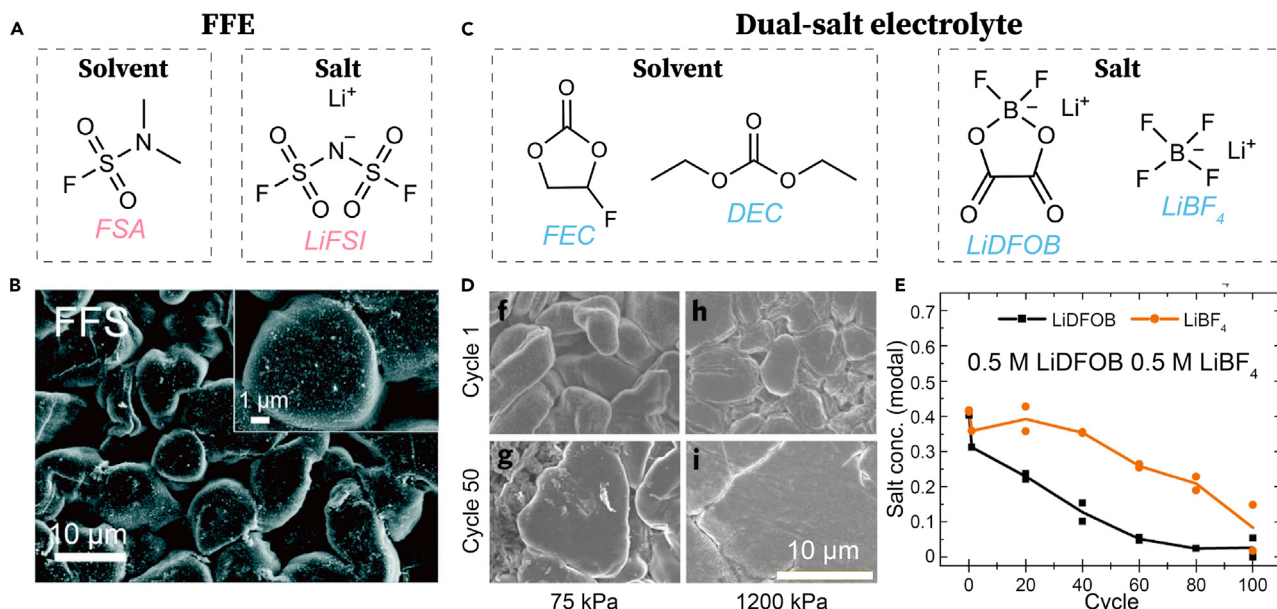
2.5) maintained 100% capacity after 200 cycles. A Cu||NMC532 industrial anode-free pouch cell maintained 80% capacity after 100 cycles. Later, shifting to the more stable fluorinated 1,6-dimethoxyhexane (FDMH) system,<sup>51</sup> an even longer cycle life was achieved with improved kinetics. The solvents in 4SEs can be not only the partially fluorinated ones, such as FDMB and FDMH, but also fluorine-free weakly solvating ones, such as 1,2-diethoxyethane (DEE) by Chen et al.<sup>62</sup> and 1,4-dioxane (1,4-DX), MTHF, and 2,5-dimethyl-tetrahydrofuran (DMeTHF) by Xu et al.<sup>91</sup> These works demonstrated the feasibility of molecular design to manipulate solvent physiochemical properties. Following this strategy, new solvent molecules are expected to be developed to further improve LMB performances.

### Fully fluorinated electrolytes (FFEs)

Increasing fluorination degree is considered generally beneficial for LMBs due to their high oxidative stability and F-rich SEI formation.<sup>52,53</sup> Therefore, the heavily or even fully fluorinated electrolyte chemistries were studied. In 2018, Fan et al. reported 1 M LiPF<sub>6</sub> in FEC-FEMC-D2 (2:6:2 by weight)<sup>52</sup> with Li metal CE of 99.2%. With the fully fluorinated electrolyte components, the highly fluorinated interphases are formed on both Li metal and high-voltage cathodes, with substantial amount of LiF. An anion-rich Li-ion environment induced by the weak solvation of highly fluorinated solvents was critical in enabling this interphase chemistry. As a result, a Li||NMC811 (2 mAh/cm<sup>2</sup>) cell with one-fold excess Li maintained 95% capacity after 120 cycles. Furthermore, the –F groups significantly improved the electrolyte non-flammability by inhibiting the oxygen radical propagation during combustion. In 2020, Xue et al. reported 1 M LiFSI in *N,N*-dimethyl-sulfamoyl fluoride (FSA)<sup>53</sup> with Li metal CE of 99.03% and fast activation within 10 cycles. This special solvent not only was fluorinated but also possessed the fluorosulfonyl group (–SO<sub>2</sub>F) resembling the FSI<sup>–</sup> anion. It was named a “full fluorosulfonyl” (FFS) electrolyte (Figure 4A). With this design, SEI primarily originated from the –SO<sub>2</sub>F decomposition, with a significant amount of LiF. This enabled uniform Li deposition morphology (Figure 4B) and improved CE. As a result, a Li||NMC622 (1.6 mAh/cm<sup>2</sup>) cell maintained 89% capacity after 200 cycles. In 2021, Xue et al. further proposed 1 M LiFSI in *N,N*-dimethyltrifluoromethane-sulfonamide (DMTMSA),<sup>67</sup> which replaced the –F group in the previous FSA solvent by a –CF<sub>3</sub> group. This design further promoted the oxidative stability of the electrolyte. A Li||NMC811 (4.86 mAh/cm<sup>2</sup>, N/P ratio = 0.39) cell cycled at 4.7 V maintained 88% of capacity after 90 cycles.

### Multi-salt electrolytes

Besides solvent, Li salts are another component of the electrolyte that can be tuned to improve the cyclability of LMBs. Promising work has combined different functionalities of two or three Li salts to simultaneously address requirements, such as Li metal compatibility and high voltage stability. In most cases, each salt in the multi-salt system possesses its unique contribution, and they function synergistically. Therefore, multi-salt systems provided more tunabilities and functionalities compared with 4SEs. In 2018, Jiao et al. reported that 2 M LiDFOB with 2 M LiTFSI in DME enabled a Li||NMC811 (1.7 mAh/cm<sup>2</sup>) cell to maintain 79% capacity after 500 cycles.<sup>68</sup> In this design, the electrolyte was superconcentrated so that the Li salts predominantly determines the interphase chemistries. LiDFOB was selected for its effect in passivating high-voltage cathodes with an insoluble, boron-rich, polymeric cathode-electrolyte interface (CEI) layer,<sup>92</sup> whereas LiTFSI was a known beneficial Li salt that promoted the formation of polymeric species –(CH<sub>2</sub>–CH<sub>2</sub>–O)<sub>n</sub>– in the SEI to protect LMAs. Qui et al. Reported a ternary-salt electrolyte using 1 M LiTFSI, 2 M LiFSI, and 3 wt % LiNO<sub>3</sub> in DME-DOL (1:1 volume ratio), enabling 99.1% CE.<sup>54</sup> In this electrolyte, LiNO<sub>3</sub> and LiFSI promoted the formation of Li<sub>2</sub>O<sup>69,93</sup> and LiF<sup>94</sup> species in the SEI respectively, whereas more stable LiTFSI salt slowed down DOL polymerization at high concentrations.

**Figure 4. FFEs and multi-salt electrolytes**

(A) Chemical composition of a “full fluorosulfonyl” electrolyte (FFS).

(B) Li deposition morphology in FFS. (A and B) Reproduced with permission.<sup>53</sup> Copyright 2020, Royal Society of Chemistry.

(C) Chemical composition of a dual-salt electrolyte.

(D) Li deposition morphology in the dual-salt electrolyte under different pressures.

(E) Salt concentration evolution results after long-term cycling. (D and E) Reproduced with permission.<sup>55</sup> Copyright 2019, Nature Publishing Group.

In 2019, Dahn and co-workers<sup>55</sup> reported 1 M LiDFOB and 0.2 M LiBF<sub>4</sub> in FEC-DEC (1:2 by volume ratio, Figures 4C and 4D), enabling an anode-free Cu||NMC532 pouch cell to retain 80% capacity after 90 cycles under a lean electrolyte condition. The authors chose LiDFOB because it promoted the LMA cycling performances, especially when combined with FEC.<sup>95-97</sup> The addition of LiBF<sub>4</sub> further improved the cell capacity retention by alleviating the fast decomposition and consumption of LiDFOB during cycling. Interphase characterization showed an increased amount of organic F species in the SEI together with inorganic LiF components. Nuclear magnetic resonance (NMR) measurement showed that both LiDFOB and LiBF<sub>4</sub> concentrations continuously decreased during cycling until full consumption (Figure 4E), whereas the solvents were mostly preserved. The authors, thus, attributed the cell failure to the loss of Li salt for ideal SEI formation and Li-ion transfer. Therefore, in follow-up works,<sup>39,56</sup> the authors increased the salt concentrations and achieved even longer cycle life. With 1.8 M LiDFOB and 0.4 M LiBF<sub>4</sub>,<sup>56</sup> a Cu||NMC532 pouch cell hot formed at 40°C lasted 195 cycles with 80% capacity retention. With even higher concentration, 2 M LiDFOB and 1.4 M LiBF<sub>4</sub>,<sup>39</sup> 200 cycles with 80% capacity retention were achieved, which represents one of the best anode-free battery cycling performances. It is worth noting that these cells were cycled between 3.6–4.5 V, so that the depth of discharge (DOD) was ~70%–80%. This enabled a Li reservoir on the Cu surface after the first cycle to compensate subsequent Li loss but would moderately undermine the battery energy.

### Electrolytes with novel additives

Electrolyte additives have long been proven to impact the performance of Li based batteries.<sup>98–100</sup> In the 1980–1990s, there were reports using 2-methylfuran<sup>101</sup> or CO<sub>2</sub><sup>102,103</sup> to improve the CE of Li. Various inorganic metal ions such as Zn<sup>2+</sup>, In<sup>3+</sup>, and Ga<sup>3+</sup> that could deposit and then alloy with metallic Li were also used as

additives.<sup>104</sup> After 2000, other metal ions, such as  $\text{Na}^+$ ,  $\text{K}^+$ , and  $\text{Mg}^{2+}$  were also explored as additives to be reduced and deposited at a higher potential than  $\text{Li}^{105-107}$  and form protective coatings. In 2013, Ding et al. reported<sup>108</sup> that the positively charged  $\text{Cs}^+$  can electrostatically shield the Li metal surface, resulting in uniform Li deposition. In 2015, Qian et al.<sup>109</sup> used water as the electrolyte additive for carbonate-based electrolytes, which led to compact nanorod-structured deposited Li. Nevertheless, even with these additives, Li metal CE rarely exceeded 95%.

During the last 5 years, various types of new organic/inorganic additives and their combinations have been explored and optimized. These additives include solvents (vinyl carbonate [VC],<sup>110,111</sup> FEC,<sup>70,111,112</sup> bis(2,2,2-trifluoroethyl) carbonate (TFEC),<sup>57</sup> etc.), salts ( $\text{LiAsF}_6$ ,<sup>110</sup>  $\text{LiPF}_6$ ,<sup>111</sup>  $\text{LiNO}_3$ ,<sup>36,70,71,93,113-115</sup>  $\text{CuF}_2$ ,<sup>71</sup> indium trifluoromethanesulfonate ( $\text{In}(\text{OTf})_3$ ),<sup>58</sup> etc.), and other materials, including  $\text{LiF}$ ,<sup>116</sup> nanodiamonds,<sup>117</sup> Li polysulfides (LiPS),<sup>36</sup> and tris(penta-fluorophenyl)borane (TPFPB).<sup>72</sup> Among them, fluorinated chemicals, such as  $\text{LiF}$ , FEC, and  $\text{CuF}_2$ , were particularly effective. Various characterization methods showed that these additives induce either  $\text{LiF}$ -rich<sup>71,112</sup> or highly homogeneous multilayered SEIs.<sup>118,119</sup> Meanwhile,  $\text{LiNO}_3$  has been broadly adopted in various works as one of the most effective additives.  $\text{NO}_3^-$  has a high cathodic decomposition potential of  $\sim 1.7$  V versus  $\text{Li}/\text{Li}^+$ , and its decomposition led to a nitrogen/ $\text{Li}_2\text{O}$  rich multilayered SEI and promoted spherical nuclei formation and homogeneous growth of Li metal with a high CE of 98%.<sup>69,113</sup> In 2018, Liu et al. reported improved CE and a  $\text{Li}||\text{NMC}111$  (8 mg/cm<sup>2</sup>) cell with over 250 cycles in a carbonate electrolyte with sustained release of  $\text{LiNO}_3$  from a polymeric membrane<sup>69</sup> (Figures 5A–5C). Combining  $\text{LiNO}_3$  with LiPS results in an even higher CE of 99.1%, which was attributed to the formation of  $\text{Li}_2\text{S}/\text{Li}_2\text{S}_2$  in the outer layer of the SEI.<sup>36</sup> However, no full-cell performance was reported due to the poor oxidative stability of the ether-based electrolyte used in this work. Combining  $\text{LiNO}_3$  with FEC in a carbonate-ether mixed electrolyte, Zhang et al.<sup>70</sup> reported a  $\text{Li}||\text{LFP}$  (2 mAh/cm<sup>2</sup>) pouch cell that maintained  $\sim 85\%$  capacity after 120 cycles. In 2019, combining  $\text{LiNO}_3$  with  $\text{CuF}_2$  in moderately concentrated 2.3 M LiFSI/DME, Yan et al.<sup>71</sup> achieved 99.5% CE and highly cyclable  $\text{Li}||\text{LFP}$  pouch cell with 4 mL/Ah of electrolyte and attributed the improved performance to the preferential absorption of  $\text{Cu}^{2+}\text{-NO}_3^-$  complexes within the inner Helmholtz plane that regulated the SEI formation.

In 2020, based on the  $\text{CuF}_2$  dissolution promoter,<sup>93</sup> Lu and co-workers<sup>58,72</sup> explored the synergistic effect of  $\text{LiNO}_3$  with Lewis-acid based additives that could coordinate with  $\text{NO}_3^-$  and help dissociate  $\text{LiNO}_3$  within carbonate-based electrolytes, where  $\text{LiNO}_3$  could barely dissolve by themselves. They combined  $\text{LiNO}_3$  with  $\text{In}(\text{OTf})_3$  in 1 M  $\text{LiPF}_6/\text{EC-DEC}$ , finding a wavy-nanostructured SEI with high content of inorganic nanocrystallites ( $\text{Li}_3\text{N}$  and  $\text{Li}_2\text{O}$ ).<sup>58</sup> A  $\text{Li}||\text{NMC}811$  (4.3 mAh/cm<sup>2</sup>) coin cell (N/P = 2.09) maintained 80% capacity after 160 cycles with 8.37 g/Ah of electrolyte. In another work,<sup>72</sup> they combined  $\text{LiNO}_3$  with TPFPB (Figures 5D and 5E) in 1 M  $\text{LiPF}_6/\text{FEC-EMC}$ , enabling a  $\text{Li}||\text{NMC}811$  (3.4 mAh/cm<sup>2</sup>) cell (N/P = 2.68) to maintain 80% capacity after 140 cycles with 3.4 g/Ah of electrolyte. TPFPB could absorb  $\text{NO}_3^-$  to reduce its abundance in the first solvation shell of Li-ions (Figure 5F). TPFPB could also decompose at the cathode surface to form F and B rich interphases, enabling the cyclability of high-voltage cathodes including LNMO. Beside these works, Wang and co-workers<sup>73</sup> reported a 0.8 M  $\text{LiPF}_6/\text{FEC-DMC}$  electrolyte with 5 wt % of 4 M  $\text{LiNO}_3/\text{DMSO}$ . Due to the high donor number of DMSO, high concentration of  $\text{LiNO}_3$  could be dissociated and incorporated into the carbonate-based electrolyte without precipitation. As a result, an inorganic-rich SEI was observed with 99.55% Li metal CE. In 2021, Sun and co-workers<sup>74</sup> reported 1 wt % of  $\text{P}_2\text{S}_5$ -saturated  $\text{CS}_2$  (PSC)

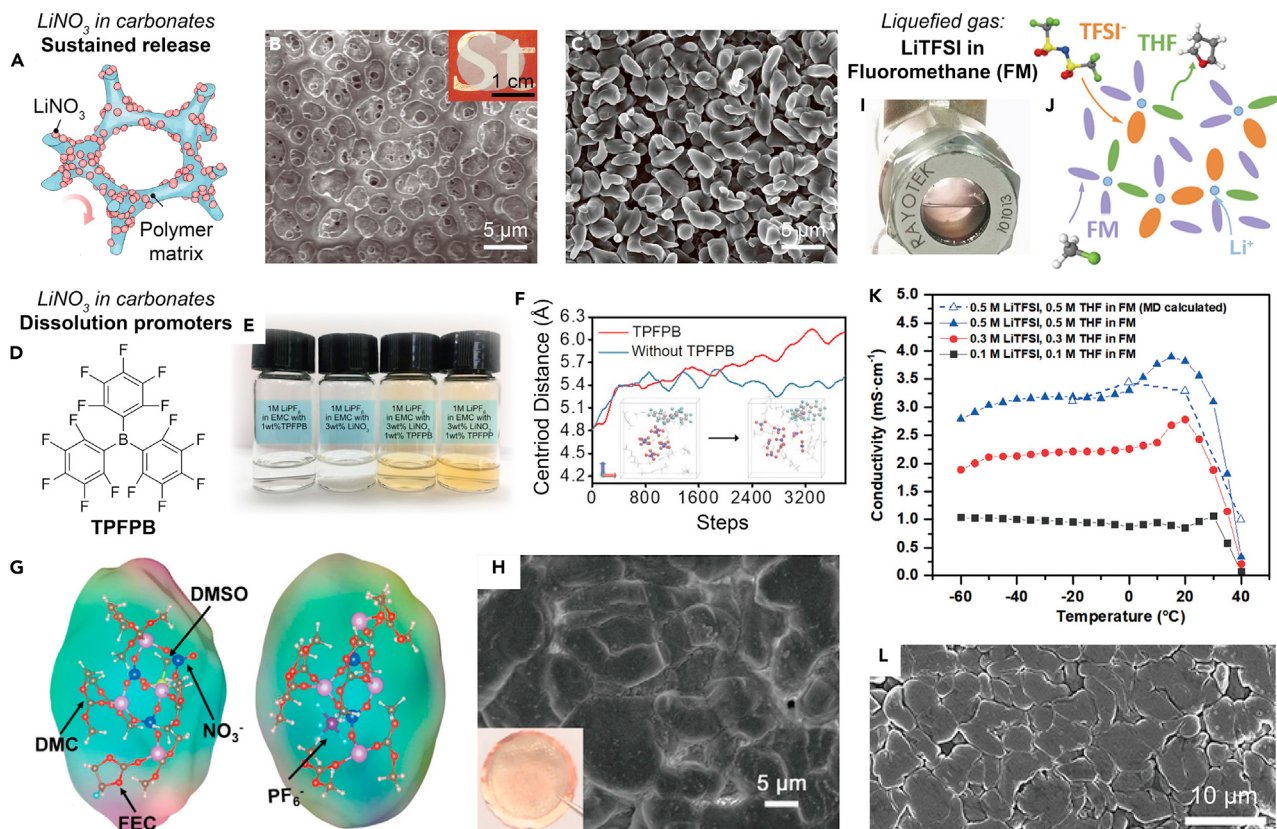


**Figure 5. Electrolytes with  $\text{LiNO}_3$  additive and liquefied gas electrolytes**

- (A) Schematic of a polymeric membrane that enables sustained  $\text{LiNO}_3$  release into the electrolyte.
- (B) SEM image of the membrane.
- (C) Li deposition morphology in 0.5 M  $\text{LiPF}_6$ /EC-DEC with  $\text{LiNO}_3$ . (A–C) Reproduced with permission.<sup>69</sup> Copyright 2018, Nature Publishing Group.
- (D) A TPFPB molecule that promotes  $\text{LiNO}_3$  dissolution in carbonate electrolytes.
- (E) Digital photo of electrolytes w/o dissolution promoters.
- (F) Simulated solvation environment in a TPFPB/ $\text{LiNO}_3$  containing electrolyte. (D–F) Reproduced with permission.<sup>72</sup> Copyright 2020, Wiley.
- (G and H) Solvation structure and Li deposition morphology in 0.8 M  $\text{LiPF}_6$ /FEC-DMC with 5 wt % of 4 M  $\text{LiNO}_3$ /DMSO. (G and H) Reproduced with permission.<sup>73</sup> Copyright 2021, Wiley.
- (I) Digital photo of a liquefied gas electrolyte 0.3 M LiTFSI-0.3 M THF/fluoromethane (FM).
- (J) Solvation environment of the liquefied gas electrolyte.
- (K) Ionic conductivity of liquefied gas electrolytes.
- (L) Li deposition morphology in 0.3 M LiTFSI-0.3 M THF/FM- $\text{CO}_2$  (19:1). (I–L) Reproduced with permission.<sup>120</sup> Copyright 2019, Elsevier.

as an additive in a carbonate-based electrolyte enabled highly ionically conductive SEI with inorganic L-P-S compounds. With this design, uniform Li deposition was realized and a  $\text{Li}||\text{NCMA}$  ( $4 \text{ mAh}/\text{cm}^2$ ) cell (N/P ratio = 5) maintained ~80% capacity after 130 cycles.

Overall, electrolyte additives have been shown to be effective, but they are likely to be gradually consumed due to repetitive SEI formation. Nevertheless, the abundance in the additive candidates and their numerous combinations and synergies still pose great potential in improving the performance of LMBs.

### Liquefied gas electrolytes

In 2017, Meng and co-workers<sup>121</sup> reported the use of gas-phase materials (under room temperature [RT]) as the electrolyte solvent for LMBs. They found the moderately polar molecule fluoromethane ( $\text{CH}_3\text{F}$ ) is gaseous at RT (boiling point:  $-78^\circ\text{C}$ )

but could liquefy and solvate LiTFSI under controlled temperature and pressure. An electrolyte composed of 0.1 M LiTFSI/CH<sub>3</sub>F showed a Li-ion conductivity of around 1 mS/cm within a broad temperature range from -60°C to 30°C. This made the electrolyte an excellent candidate for low-temperature batteries. Meanwhile, when the temperature surpassed ~40°C, salt precipitated to trigger a severe drop in ionic conductivity, which could be utilized to shut down batteries during thermal runaways. With a further optimized electrolyte formulation 0.2 M LiTFSI/CH<sub>3</sub>F-CO<sub>2</sub> (19:1), an LCO cathode could normally cycle under -40°C. Furthermore, Li metal showed a CE of 97% within this electrolyte, which was attributed to the LiF and LiCO<sub>3</sub> rich SEI from solvent decomposition. In a follow-up work,<sup>120</sup> the LiTFSI solubility was improved by adding THF as a co-solvent. With an optimized formulation 0.3 M LiTFSI-0.3 M THF/CH<sub>3</sub>F-CO<sub>2</sub> (19:1, Figures 5I and 5J), the ionic conductivity was further increased to ~2 mS/cm (Figure 5K) with excellent performance at low temperature. This modified electrolyte also promoted a Li metal CE of 99.6% because of the highly uniform and dense Li deposition pattern (Figures 5L and 5M). A Li<sub>4</sub>Ti<sub>5</sub>O<sub>12</sub>-LiNi<sub>0.8</sub>Co<sub>0.15</sub>Al<sub>0.05</sub>O<sub>2</sub> (LTO/NCA) 18650-type full cell was demonstrated for 35 cycles using this electrolyte. In another follow-up work,<sup>122</sup> liquefied LiTFSI/AN-CH<sub>3</sub>F was also demonstrated to be effective in LMBs. Overall, liquefied gas electrolytes could significantly promote the low-temperature performances and safety of both LIBs and LMBs, but their long-term cycling stability requires further verifications and the challenges they pose to battery manufacturing needs to be fully addressed for practical applications.

### KEY FEATURES ENABLED BY ADVANCED LMB ELECTROLYTES

To achieve a practical LMB, the electrolyte must be compatible with both LMAs and high-voltage cathodes. On the anode side, to achieve an Li metal cycling CE over 99.5%, two sources of Li loss need to be suppressed: "dead Li" and SEI formation.<sup>37</sup> On the cathode side, the electrolyte must possess reasonable oxidative stability. In this section, we try to summarize the key features of recent high-performing electrolytes to meet the requirements above.

#### Fluorine chemistry

Fluorinated molecules have become increasingly critical in advanced LMB electrolytes. Fluorine is the most electronegative element; therefore, functionalization of solvent molecules with strongly electron-withdrawing -F groups can significantly enhance their oxidative stabilities. This is particularly important for ether-based solvents that are beneficial for LMAs but generally have poor stability toward cathodes.<sup>32</sup> In the past 5 years, a series of fluorinated ether molecules were explored to enable advanced LMB electrolytes, especially for the LHCE strategy. The electron-withdrawing nature of -F group typically weakens the polarity of the solvating groups that interact with Li<sup>+</sup>, enabling effectively non-solvating diluents. These diluent molecules included BTFE,<sup>63</sup> TTE,<sup>50</sup> TFEO,<sup>42</sup> D2, M3,<sup>90</sup> etc. However, the choices were limited by commercial availability so that other properties, such as Li-ion solvability, could not be finely tuned at will. In 2020, Yu and co-workers<sup>35</sup> designed a new molecule (FDMB) and its analogs. The rationally designed solvent molecules enabled excellent oxidative stability and tunable Li-ion solvability through selected-site fluorination. This work shows the methodology of designing fluorinated solvent molecules for practical LMBs.

#### Non-dendritic Li deposition morphology

Homogeneous Li deposition morphology with large Li granular sizes is a necessity for high Li metal CE. Large Li granules with low aspect ratio and tortuosity minimize "dead Li" formation during Li stripping.<sup>37,38</sup> Furthermore, larger grain sizes lead to

reduced surface area, which could minimize SEI formation. Within recent advanced LMB electrolytes, non-dendritic, chunky Li deposition was commonly observed, although with slightly different morphological features. In HCEs, such as 4 M LiFSI/DME,<sup>34</sup> the deposited Li was described as “nodule-like particles with round-shaped edges and ~10 μm sizes” (Figure 3C). In LHCEs, such as 1LiFSI-1.2DME-3TTE, “quite uniform large Li deposits formed”<sup>50</sup> and their morphology seemed slightly chunkier with even lower porosity than that in the HCE (Figure 3E). Various electrolytes with LiNO<sub>3</sub> additive were found to enable spherical-shaped Li nuclei<sup>123</sup> that “evolve into nodule-like shapes under increased capacities.”<sup>69</sup> In the recently reported 1 M LiFSI/FDMB, Li showed “densely packed, flat, large grains”<sup>35</sup> (Figure 3H). In the dual-salt LiDFOB/LiBF<sub>4</sub> electrolyte systems, Dahn and co-workers reported a “dendrite-free, close packed”<sup>55</sup> Li morphology (Figure 4E). With a high operational pressure of 1,200 kPa, this electrolyte resulted in a “smooth Li mosaic comprised of densely packed domains up to 50 μm.”<sup>55</sup> The fundamental origin of these similarly uniform Li depositions within different advanced electrolytes is still not fully understood, but they were generally attributed to the altered SEI chemical/structural uniformity and growth rate.

### SEI microstructure and homogeneity

With the development of cryogenic electron microscopy (Cryo-EM) technology, highly sensitive materials, such as metallic Li and SEIs, were characterizable at high resolutions.<sup>119,124,125</sup> Li et al.<sup>119</sup> reported the evolution from a mosaic<sup>126</sup> to a multi-layered<sup>127</sup> SEI microstructure after the addition of FEC to 1 M LiPF<sub>6</sub>/EC-DEC electrolyte (Figures 6A and 6B). In a follow-up work,<sup>118</sup> mosaic SEIs were shown to have high crystallinity “hot-spots” with higher ionic conductivity, which led to aggravated “dead Li” formation during stripping. In contrast, the improved structural homogeneity of multilayered SEIs improved the CE. Cryo-EM was then applied to examine the SEI for several advanced LMB electrolytes. In a LHCE electrolyte (1 M LiFSI/DME-TFEO), Cao et al.<sup>42</sup> described the SEI as “monolithic,” because it possessed no crystalline domains and had a consistent thickness of ~10 nm (Figures 6C and 6D). Together with XPS results, this SEI was shown to be uniform in both its thickness and its chemical composition. A similar SEI was observed for 1 M LiFSI/FDMB<sup>35</sup> where the SEI thickness was ~6 nm (Figure 6F), much thinner than that in 1 M LiFSI/DME (~10 nm)<sup>35</sup> (Figure 6E) and carbonate electrolytes (15–20 nm).<sup>119</sup> Furthermore, the SEI was highly uniform, in contrast to that in 1 M LiFSI/DME containing wrinkles. In summary, advanced electrolytes generally enable thin, fully amorphous, and highly homogeneous SEIs.

### SEI chemistry and Li-ion solvation environments

The chemical components of SEIs determine critical properties such as ionic conductivity<sup>118</sup> and interfacial energy,<sup>128</sup> thus, impacting Li deposition morphology and CE. The importance of SEI chemistry can be traced back to the Li-ion solvation structure, because the composition of the first solvation shells directly determines the chemical content of the SEI. In this section, we categorize and discuss the common SEI chemistries observed in advanced LMB electrolytes and their origins from the perspective of Li-ion solvation environments.

#### Inorganic-rich SEIs

SEIs formed in baseline carbonate electrolytes typically exhibit highly organic nature<sup>42,50,52</sup> with ~40% atomic ratio of carbon on the surface of deposited Li (Figure 7A). This is because carbonate solvents coordinate strongly with Li-ions,<sup>129,130</sup> and they significantly decompose during Li deposition. By replacing carbonates with weaker solvating ethers,<sup>42</sup> such as DME, the carbon ratio within SEIs slightly decreased to ~20% (Figure 7B) due to less solvent decomposition.

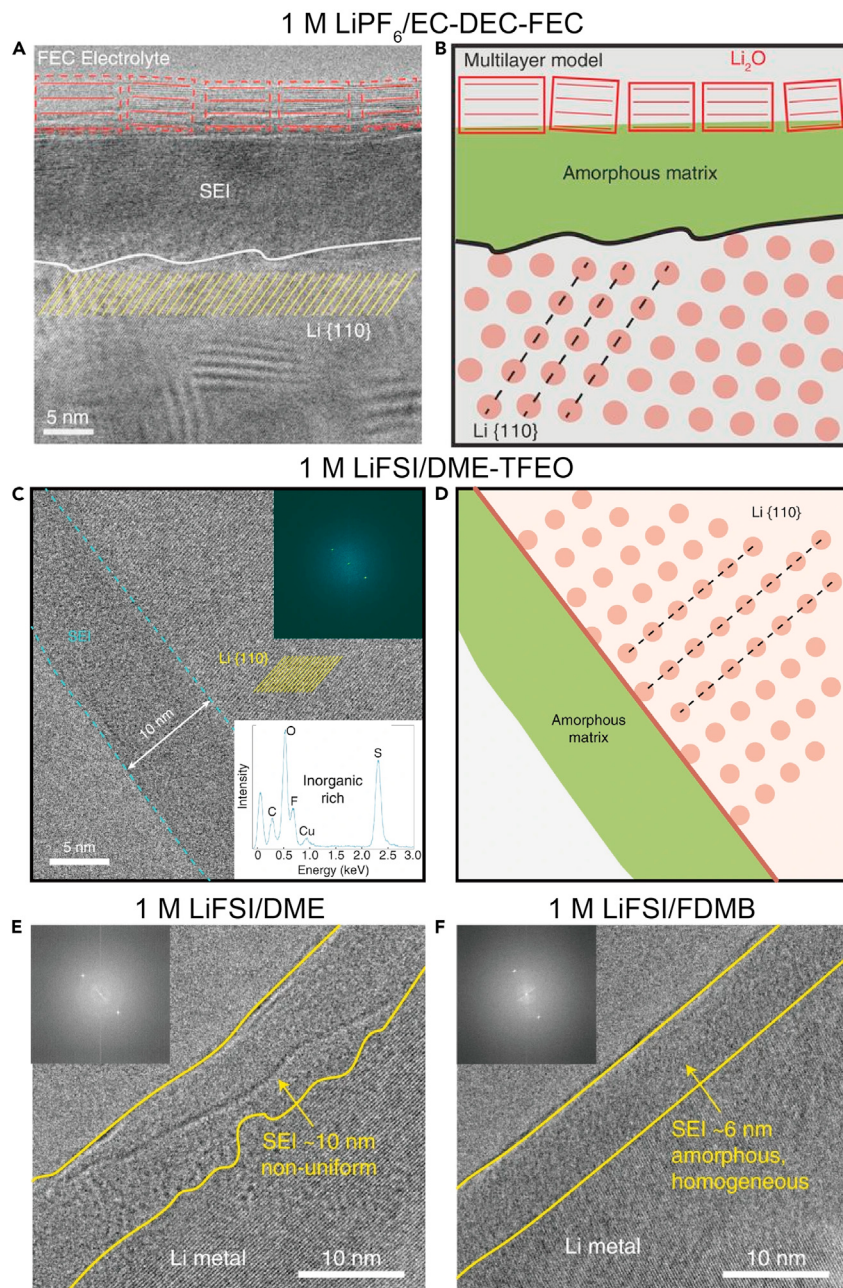


**Figure 6. Cryo-EM characterized SEI microstructures**

(A) Image of the Li SEI in 1 M LiPF<sub>6</sub>/EC-DEC-FEC.

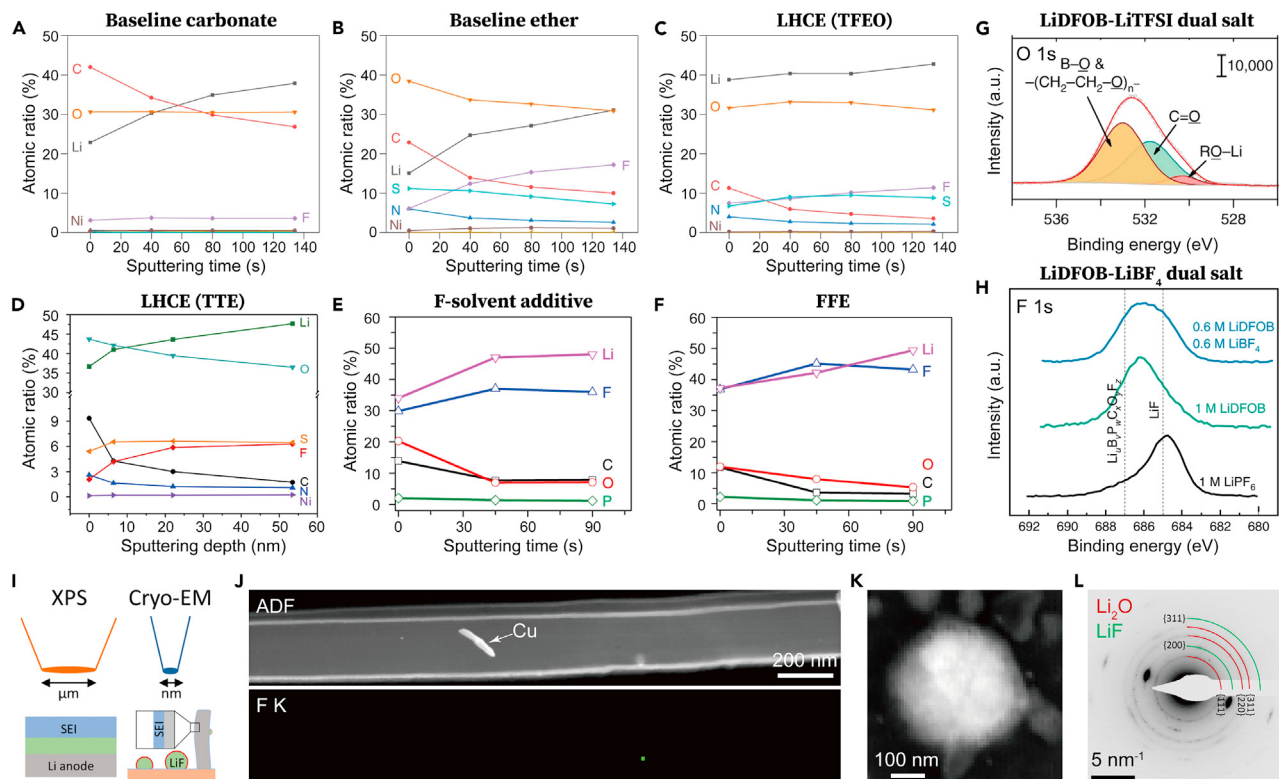
(B) Schematic illustration of (A). (A and B) Reproduced with permission.<sup>119</sup> Copyright 2017, American Association for the Advancement of Science.

(C) Image of the Li SEI in 1 M LiFSI/DME-TFEO.

(D) Schematic illustration of (C). (C and D) Reproduced with permission.<sup>42</sup> Copyright 2019, Nature Publishing Group.

(E) Image of the Li SEI in 1 M LiFSI/DME.

(F) Image of the Li SEI in 1 M LiFSI/FDMB. (E and F) Reproduced with permission.<sup>35</sup> Copyright 2020, Nature Publishing Group.

**Figure 7. SEI chemistries**

(A–F) XPS depth profile of the elemental ratio within the surfaces of Li deposited in: 1 M LiPF<sub>6</sub>/EC-EMC-2%VC (A), 1 M LiTFSI/DME (B), 1 M LiTFSI/DME-TFEO (C), 1LiTFSI-1.2DME-3TTE (D), 1 M LiPF<sub>6</sub>/DME-FEC (E), 1 M LiPF<sub>6</sub>/FEC-FEMC-D2 (F). (A–C) Reproduced with permission.<sup>42</sup> Copyright 2019, Nature Publishing Group. (D) Reproduced with permission.<sup>50</sup> Copyright 2019, Elsevier. (E and F) Reproduced with permission.<sup>52</sup> Copyright 2018, Nature Publishing Group.

(G) XPS O 1s spectra of Li deposited in 2 M LiTFSI-2 M LiDFOB/DME dual-salt electrolyte. Reproduced with permission.<sup>68</sup> Copyright 2018, Nature Publishing Group.

(H) XPS F 1s spectra of Li deposited in a LiDFOB-LiBF<sub>4</sub>/FEC-DEC dual-salt electrolyte. Reproduced with permission.<sup>55</sup> Copyright 2019, Nature Publishing Group.

(I) Schematic showing the difference between XPS and Cryo-EM characterizations on SEI chemistry.

(J) Cryo-STEM EELS mapping a Li filament with a single LiF particle.

(K) Cryo-STEM ADF image of LiF nanoparticle formed on the TEM grid electrode surface.

(L) SAED pattern of a LiF particle. LiF and Li<sub>2</sub>O reflections are visible. (I–L) Reproduced with permission.<sup>131,132</sup> Copyright 2020 and 2021, American Chemical Society.

In contrast, more inorganic compositions in SEIs were observed within most advanced LMB electrolytes. For HCEs and LHCEs, the inorganic SEI chemistry was attributed to the anion-rich Li-ion solvation environments. For example, with 4 M LiTFSI/DME,<sup>34</sup> researchers showed through theoretical modeling that only 3% of FSI<sup>-</sup> anions were uncoordinated and only 6% of Li-ions were solely solvated by DME. This led to an inorganic-rich SEI dominated by anion decomposition, instead of a SEI that was rich in ether reduction products, such as ROLi.<sup>34</sup> Such a SEI chemistry also appeared in LHCEs, because the incorporation of diluents barely altered the Li-ion solvation environments. In 1 M LiTFSI/DME-TFEO<sup>42</sup> and 1LiTFSI-1.2DME-3TTE,<sup>50</sup> the SEIs were observed to be rich in -SO<sub>2</sub>F and -SO<sub>x</sub> functional groups and other inorganic components, such as LiF, Li<sub>2</sub>S, and Li<sub>3</sub>N. Carbon ratio was shown to be below 10% in both electrolytes (Figures 7C and 7D), confirming the inorganic nature of SEIs. Similar SEI chemistry was also observed for 1 M LiTFSI/FDME,<sup>35</sup> where the average anion/solvent ratio increased to ~3.29 compared with ~2.31 in 1 M LiTFSI/DME. In these cases, the anion-rich Li-ion solvation

environments originate from the incorporation of weakly solvating molecules, which are usually fluorinated ethers. The electron-withdrawing effect of fluorine could weaken the coordinating capability of solvents' oxygen atoms toward Li-ions, leading to enhanced ion pairing. Besides this approach, another way to enable inorganic-rich SEIs is to use solvents with inorganic decomposition products. Fan et al. showed that the addition of FEC into baseline carbonate electrolyte could reduce the carbon ratio in SEIs to ~10% (Figure 7E),<sup>52</sup> together with significantly enhanced fluorine species originated from FEC decomposition. By completely replacing the baseline carbonates with fluorinated solvents, carbon ratio in the SEI was further reduced to below 10% (Figure 7F). Overall, inorganic-rich SEIs are observed in most advanced LMB electrolytes and considered critical for an improved LMA cycling performance.

#### *Organic-rich SEIs*

Organic-rich SEIs were rarely found to enhance LMA performances and mostly reported in dual-salt electrolytes with LiDFOB as the Li salt. One example was 2 M LiDFOB-2 M LiTFSI/DME. Through a series of characterizations, Jiao and co-workers<sup>68</sup> observed enrichment in  $-(\text{CH}_2-\text{CH}_2-\text{O})_n-$  (Figure 7G) and attributed this to the cross-linking or polymerization reactions induced by the electron-deficient state B atoms after B-O bond breakage. Another example was the dual-salt LiDFOB/LiBF<sub>4</sub> electrolyte reported by Dahn and co-workers.<sup>55</sup> XPS analysis of the F 1s fine structure showed that the SEI formed with LiPF<sub>6</sub> was predominantly composed of LiF, whereas that formed with LiDFOB mostly consisted of organic F species (Figure 7H). In the dual-salt LiDFOB/LiBF<sub>4</sub> electrolytes, equally strong signals were observed for LiF and organic F, which was considered responsible for its excellent performance in LMBs.

#### *Where is LiF?*

LiF is an almost universally observable SEI component in both conventional and advanced electrolytes and considered critical for Li metal cyclability.<sup>52,112,116</sup> In previous studies, LiF was predominantly observed via XPS F 1s peak assignments. However, a discrepancy on where LiF is located emerged when Cryo-EM results showed the absence of LiF within the compact SEIs in various electrolytes.<sup>35,42,69,113,119</sup> This discrepancy was resolved when the different spatial resolutions of XPS and Cryo-EM were taken into consideration (Figure 7I). The in-plane spatial resolution of XPS is limited to micrometer scale, meaning that the spectra represent signals from a  $\mu\text{m}$ -sized area with not only Li grains but also other particles dispersed on their surfaces. Through Cryo-EM and electron diffraction characterizations on a TEM grid electrode, Huang et al.<sup>131,132</sup> discovered that LiF deposited as crystalline nanoparticles with  $\sim$ 100–400 nm sizes on the current collector and, sparsely, on Li metal (Figures 7J–7L). These LiF nanoparticles were likely the origin of the LiF signals observed in the XPS characterizations. A similar morphology of LiF was also observed by Jurng et al.<sup>96</sup> Because LiF did not appear in compact SEIs that were in direct contact with Li metal, it was termed as an indirect SEI.<sup>131,132</sup> Consequently, LiF may not serve a crucial role in Li direct surface passivation as proposed previously.<sup>52,112</sup> However, the high surface energy and low Li adatom surface diffusion barrier<sup>47,116</sup> of LiF might still play a role in promoting horizontal Li deposition. Further studies directly correlating the spatial distribution of LiF to the morphology of electrodeposited Li deposition are required to fully reveal the role of LiF in Li metal cycling.

## FUTURE DESIGN AND METRICS FOR ADVANCED LMB ELECTROLYTES

Although various strategies of electrolyte engineering have been reported before and summarized above, wide space still exists for the development of next-generation liquid

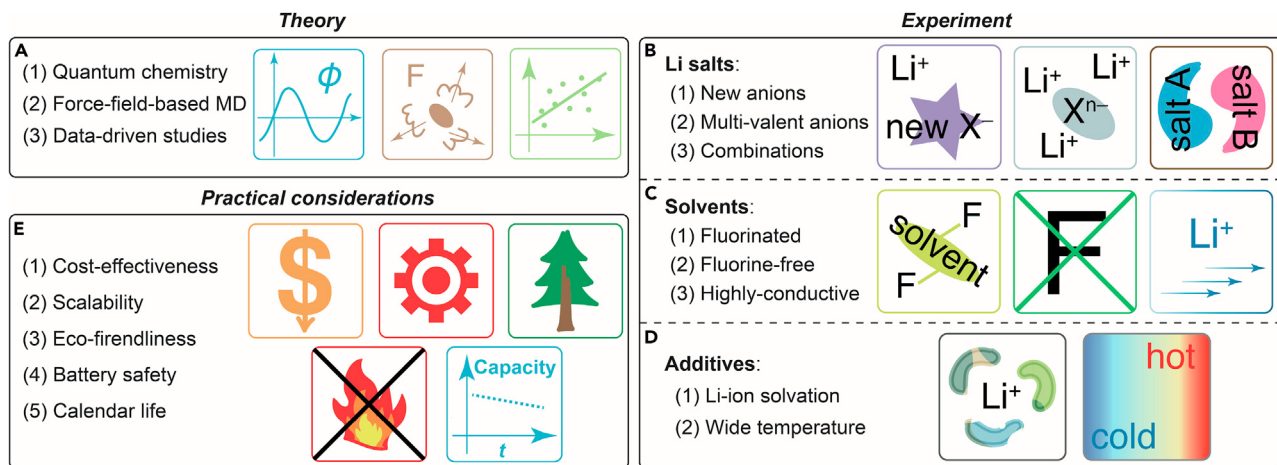


**Figure 8.** Future directions for LMB electrolyte research

(A) Design inspired by theoretical models: quantum chemistry, molecular dynamics and data-driven analysis.

(B–D) Experimental efforts on the electrolyte components, which are Li salts, solvents, and additives, under the guidance of theories.

(E) Important practical considerations beyond novel experimental advancements.

electrolytes. Both experimental and theoretical efforts are needed and, herein, we provide potential directions for exploring future electrolytes.

### Theoretical simulations and data-driven studies

#### Theoretical simulations

A battery is a complex system composed of various components, including the anode, cathode, electrolyte, and SEI. The multiscale processes in batteries are further complicated by mass transport and side reactions.<sup>133</sup> All of these factors render it nontrivial, if not impossible, to design Li electrolytes following a few principles or using only one theoretical or simulation tool. Nevertheless, molecular simulations at different levels can provide essential insights about different processes in a battery.<sup>134</sup> Simulation should, therefore, be utilized as a critical tool in guiding the future development of advanced LMB electrolytes (Figure 8A).

Quantum chemistry calculations at different levels (semi-empirical methods, density functional theory, and wave function level) are usually adopted to gather single-molecule information of electrolyte components. Representative quantities include the HOMO, LUMO, ionization potential, and electron affinity of individual electrolyte components.<sup>135</sup> They provide key properties of electrolyte components without performing detailed and expensive condensed-phase simulations. These quantities from quantum calculations can give decent estimations of many important properties, such as electrochemical window, solubility of Li-ions, and reductive/oxidative stability. Therefore, high-throughput quantum calculations are a powerful method for screening candidate electrolytes from a pool of possible components.<sup>136–139</sup> Furthermore, quantum calculations based on clusters can also predict the interaction between Li-ions and other electrolyte components.<sup>140</sup> Infrared spectroscopy and NMR shifts from cluster calculations can be used to compare with and explain experimental data to gather more insights about the Li-ion solvation environments<sup>141</sup> in advanced electrolytes.

Force-field-based MD simulations can simulate electrolytes at larger scales of up to tens of nanometers, which makes the study of bulk electrolyte properties possible. The

solvation structure around each Li-ion can be obtained explicitly in these types of simulations.<sup>141,142</sup> Besides thermodynamic properties, MD simulations can also be used to study dynamic properties,<sup>142,143</sup> such as viscosity, dielectric relaxation, diffusivity, and ionic conductivity. Therefore, MD is a powerful tool for obtaining insights about the roles of different electrolyte components on key properties of advanced electrolytes. Additionally, MD simulations based on *ab initio* methods<sup>144,145</sup> or reactive force fields<sup>146,147</sup> can also shed light on the evolution of SEI. This makes it a promising method to reveal and rationalize the special interfacial properties enabled by advanced electrolytes, guiding further electrolyte formulation optimizations.

#### *Data-driven studies*

Recently, data-driven analysis and design have revealed great potential for battery developments.<sup>139,148–151</sup> Sendek et al. developed a machine learning (ML) model that predicted ionic conductivity of solid state electrolytes for LMBs based on quantum calculation data.<sup>152</sup> Attia et al. developed a model that can predict the cycle life of batteries from voltage profiles of the first 100 cycles<sup>153</sup> and further used the model to obtain the optimal fast-charging protocol through a closed-loop optimization process.<sup>154</sup> Despite the liquid electrolyte formulations developed for LMBs, there remains a vast and largely unexplored chemical design space, providing opportunities to use data-driven analysis. High-throughput screening of electrolytes through calculations, combined with data-driven approaches, can make electrolyte discovery more accessible (Figure 8A).

Two types of approaches can potentially be adopted to optimize the LMB electrolyte formulation. First, theoretical simulation data can be utilized to predict electrolyte properties through a bottom-up manner. Specifically, calculated properties, such as HOMO/LUMO quantities and solvation structures, can be fed into ML models, which can be subsequently used to guide electrolyte designs. On the other hand, a top-down approach can also be adopted. Experimental data, such as CE or full-cell cycle life, could be used to train a ML model to extract the key features (such as chemical compositions) of a certain electrolyte that determine its performance. If these approaches are successful, future experimental screening of the electrolyte can be accelerated.

#### **Molecular designs for LMB electrolytes**

Recent works on electrolyte engineering usually focused on tuning the recipe with commercialized chemicals. While this progress is undoubtably critical and worth exploring,<sup>98,99,155,156</sup> we believe that an important future direction is to develop rationally designed structures and to explore new chemicals. Organic and inorganic synthetic methodologies, therefore, can be the central tools in the next phase of electrolyte research. This section is categorized by common components in liquid electrolytes, i.e., Li salts, solvents, and additives, and an outlook is provided for each component.

#### *Li salts*

As the source of Li-ion transport, Li salts are critical for advanced electrolytes.<sup>157</sup> Three potential directions for developing Li salts are (1) new-anion salts, (2) multivalent anions, and (3) combination of different salts (Figure 8B).

The anion of the Li salt determines the quality of SEI and, as a result, the CE. Therefore, opportunities exist for designs of Li salts based on novel anions to fulfill the urgent demand for higher Li efficiency. For example, promising candidates include recently rising Hückel-type anions, such as 4,5-dicyano-2-(trifluoromethyl)imidazole (TDI) and 4,5-dicyano-2-pentafluoroethylimidazolate (PDI),<sup>158</sup> fluorinated

phosphates, such as difluorophosphate (DFP),<sup>159,160</sup>  $[\text{PF}_3(\text{CF}_2\text{CF}_3)_3]^-$  (FAP),<sup>161</sup> tetra-fluoro oxalato phosphate (TFOP),<sup>162</sup> various fluorosulfonyl imides,<sup>163–167</sup> new borates,<sup>168–170</sup> acetates,<sup>171</sup> and even fluorine-free anions, such as  $\text{AlCl}_4^-$ ,<sup>172</sup> and cyano-based anions.<sup>158,173,174</sup>

Despite these novel yet monovalent anions, one can further create multivalent anions for Li salts to enhance the Li-ion density and salt utilization by reducing the anion/cation ratio. For example, several divalent fluorosulfonyl imide-based salts were proposed and synthesized.<sup>175,176</sup> It is worth noting, however, that multivalent anions may also introduce poor solubility; therefore, fine tuning of the size and substitution of multivalent anions can be applied to enable decent salt dissolution. Another potential issue to be considered is the strong electrostatic interaction between multivalent anions and Li cations, which may negatively affect the transport properties.

Besides the design and synthetic efforts mentioned above, perfect recipes for different Li salts (i.e., multi-salt approach as elaborated above) can be a supplemental approach to synergically boost Li metal performance. Combinations of both existing salts with synthesized salts can be pursued. This point is even more critical if the synthetic salts are less cost-effective or scalable than commercially available ones.

#### *Electrolyte solvents*

Physicochemical properties of electrolyte solvents are crucial to LMBs.<sup>26,177</sup> The solvent should also be stable toward cathodes, but, herein, we mainly focus on the general design directions for electrolyte solvents that are stable toward LMAs: (1) new fluorinated solvents, (2) fluorine-free eco-friendly solvents, (3) highly conductive solvents, (4) non-flammable/safe solvents, and (5) combination of different solvents (Figure 8C).

Fluorine is a well-known “magic” element to stabilize LMBs.<sup>178,179</sup> Although a number of fluorinated solvents and diluents have been reported (e.g., fluoro-carbonates,<sup>52,177,180,181</sup> fluoro-esters,<sup>177,182</sup> fluoro-acetamide,<sup>183</sup> fluoro-sulfonamide,<sup>53,67</sup> fluoro-ethers,<sup>32,35,42,184,185</sup> fluoro-phosphates,<sup>186–188</sup> fluoro-sulfones,<sup>189,190</sup> fluoroalkanes,<sup>121</sup> fluorinated aromatic diluents,<sup>191,192</sup> fluorinated ionic liquids,<sup>193</sup> etc.), few newly synthesized compounds have been applied to LMBs. Opportunities exist to take the advantage of organic synthetic tools to explore novel small molecules as electrolyte solvents or diluents. Another direction in need is deeper understandings of the structure-property relationships between fluorination sites on the molecules and impact on battery performance. Particularly, the effect of electrostatic/non-covalent Li–O and/or Li–F interactions on solvation structure and overall performance deserves further exploration.

Besides fluorinated solvents, an opposite yet promising approach is fluorine-free solvents. Eliminating fluorine atoms in solvent molecules will have profound impacts for eco-friendliness.<sup>173,174,194</sup> The challenge is to maintain or even enhance the battery performance while removing fluorine substitutions. One promising and recently explored direction is to construct steric molecules to enable weakly solvating solvents for better Li metal stability.<sup>62,91,195</sup>

Solvents with great salt solubility and high ionic conductivity are essential for fast-charging capabilities and low-temperature operation of LMBs. Special solvation environments tailored by the electrolyte design can modulate the charge transfer process to enable low-temperature cyclability.<sup>196</sup> Nevertheless, the molecular-level design principles of solvent structures remain elusive in this field. One may

learn from the electrolyte design for fast charging and low-temperature cycling of LIBs,<sup>197</sup> and modify the solvents, such as esters and nitriles, as well as ethers, according to the requirements of LMBs.

Similar to Li salts, solvents can also be mixed for an ideal formulation. Combinations of the fluorinated solvents, diluents, fluorine-free solvents, and highly conductive and non-flammable solvents (as will be discussed in the later Battery safety section) may yield synergistic effects and improve the CE of Li metal.

#### Additives

Additives make up small proportions of the electrolyte, but they can dramatically affect the performance of LMAs.<sup>100</sup> Countless additives have been reported, and further development should expand beyond the salts and solvents mentioned above. While the functioning path of an additive may vary, its most important roles are (1) tuning SEI and Li<sup>+</sup> solvation structure for better Li metal CE, and (2) enabling a wide range of temperatures for battery operation (Figure 8D).

Additives can tune the SEI in several ways<sup>198</sup>: (1) an additive itself decomposes on Li metal and forms stable products in SEI, (2) an additive modifies the solvation structure and renders preferential decomposition of other components to form a stable SEI, or (3) synergistic function of (1) and (2). Regardless of the detailed mechanism, the target is to create a more stable SEI on LMAs. Systematic studies on the structure-property relations between additive structure and SEI quality is lacking, and upgrading existing additives, such as LiNO<sub>3</sub>, is an urgent direction. Research into the effect of different dissolution promoters on cycling efficiency are needed, which will benefit further design of novel promoter structures. In the meantime, other novel additives to further improve SEI quality and boost Li metal performance can be designed and obtained through cost-effective and large-scale synthesis. Additives for wide temperature operation will be discussed in the later section.

#### Practical considerations for LMB electrolytes

In addition to the above materials and chemistry-based outlooks, we need to pay attention to the practicality of electrolyte strategies from the perspectives of industry, consumers, and market. Detailed categories and elaborations are as follows.

##### *Cost-effectiveness, scalability, and eco-friendliness*

The manufacturing cost is a critical consideration for the commercialization of LMBs, so designs of new Li salts, solvents, and additives must consider the cost-effectiveness of an electrolyte. The price of starting reagents, the step length of synthetic procedures, the cost of reaction conditions and purification (e.g., strict and harsh conditions increase the cost), and the yield of products (Figure 8E) are important components of the cost and determine the intrinsic scalability of the electrolyte. Electrolytes account for ~15% cost of the whole Li-ion battery, and it is safe to expect higher cost for electrolytes in LMBs due to the use of more expensive Li salts and newly synthesized solvents or additives.<sup>26,157,199</sup> It is noteworthy that the mass production of conventional carbonate electrolytes over the past decades significantly optimized the synthetic pathways so that the cost could be reduced. This means that recent advanced electrolytes do have significant space for cost reduction if put into mass production, and this still reminds us to prioritize cost-effectiveness during electrolyte designing.

Moreover, green chemistry and atom economy should be applied to mitigate or even eliminate the pollution generated during battery chemical manufacturing.<sup>26</sup> For example, organic-solvent-free method such as ball milling can be implemented

in salt synthesis,<sup>159</sup> whereas organic synthetic procedure can be designed to generate fewer side products. All these require the manufacturing and engineering efforts from chemical industry.

#### Battery safety

Safety is another critical concern in realistic LMBs for consumers, so non-flammable solvents and/or additives with optimized battery performance are worth developing. Generally, phosphates, sulfones, and fluorine-rich solvents are fire retardant, but they often have poor Li metal CE.<sup>52,66,85,186,200</sup> Post-modification of these chemicals can be conducted to improve their cycling performance while retaining the non-flammability. The incorporation of special additives containing halogen or phosphorus elements can mitigate flammability as well.<sup>100</sup> It is noteworthy that battery safety is complex and should be examined within commercial level cells under realistic testing conditions including nailing tests or heating,<sup>39,201</sup> because thermal runaway is related to factors beyond solvent flammability, such as exothermic reactions between electrolyte components and electrodes and the subsequent gassing issue.<sup>39,201</sup> In a recent report,<sup>201</sup> Ouyang et al. found that even the HCE based on fire-extinguishing solvent, trimethyl phosphate (TMP), would catch fire under a nailing test, although it had been assumed non-flammable for long. This new learning calls for more practical and careful examination for LMB safety when using advanced electrolytes.

#### Calendar life

Recent developments of LMB electrolytes particularly emphasize the improvement in battery cycle life, whereas they place less attention on the cell calendar life (capacity retention after storage at open circuit), which is equally critical for the commercialization of LMBs. Although advanced LMB electrolytes have dramatically enhanced the cycling efficiency, full-cell calendar life is still not satisfying.<sup>202,203</sup> Specifically, Boyle et al. found that advanced electrolytes that enabled long LMB cycle life demonstrated similar calendaring aging rates as conventional electrolytes.<sup>202</sup> This indicates that enhancement of cycle and calendar life follows distinct mechanisms. High cycling efficiencies can be accomplished through the promotion of large Li deposition granules that minimizes "dead Li" formation.<sup>37</sup> During calendar aging, however, thickening of SEIs and even the formation of extended SEIs were observed for various electrolytes and considered as the dominant source of capacity loss.<sup>202</sup> Therefore, achieving satisfying calendar life requires more emphasis on the passivation of Li with SEI. Consequently, future advanced LMB electrolytes are required to not only enable low surface area of deposited Li, but also promote highly passivating SEIs with stable chemical components and dense microstructures that are non-permeable to electrolytes. One possible direction that has been found is to introduce LiNO<sub>3</sub> additive that effectively passivated the Li surface during calendar aging.<sup>202</sup> The designs for long calendar life electrolytes may be enabled in the future by further and deeper understandings on Li-ion solvation and the corresponding SEI formation pathways. Moreover, the calendar life needs to be verified with full-cell configurations under industry standards, because cathodes and realistic cycling conditions matter as well in calendar aging.

#### Wide temperature range operation

Another important yet less-studied area is the electrolytes to enable wide temperature operation of LMBs, which can be achieved through tuning of SEI and Li-ion solvation structure. Generally, low-temperature cycling requires highly conductive SEIs and lower de-solvation barrier,<sup>18,90,182</sup> whereas high-temperature performance depends more on the robustness of SEI and CEI.<sup>113</sup> The latter direction is less studied in LMB field, although several reports on LIBs showed unsaturated bonds on phosphate<sup>204</sup> or silane<sup>205</sup> structures helped with cycling at elevated temperatures.

Some novel salts<sup>113,168</sup> and a conventional electrolyte 1 M LiTFSI/DOL-DME with LiNO<sub>3</sub> additive<sup>113</sup> have been found to enable better cycling of high-temperature LMBs, but the molecular design methodology for high-temperature LMB additives is missing. On the other hand, the low-temperature operation of LMBs is attracting research attention due to the demand of running electric vehicles in cold weather. Several examples such as liquified gas electrolytes,<sup>120</sup> weakly solvating solvent<sup>196</sup> and all-fluorinated solvents<sup>90,182</sup> have been demonstrated to enable stable cycling of LMBs under extremely low temperature up to -95°C; however, some of them suffer from low boiling point, limiting their practical applications at room temperature. Therefore, systematic studies and more molecular designs are still needed for future low-temperature electrolytes.

### Critical metrics for evaluating developed electrolytes

It is critical for the community to agree on a set of standardized criteria for evaluating the performance of electrolytes. Several journals announced the checklists<sup>206,207</sup> for experimental battery research and these can be good practices to implement into electrolyte works. We suggest that critical cell conditions need to be clearly and directly stated in the figure plots, figure captions, tables, or methods section. These critical parameters include: (1) Li metal thickness or Li inventory amount, (2) cathode type, loading, active material/conductive carbon/binder ratio, (3) electrolyte amount, i.e., E/C ratio, (4) cycling conditions such as charge/discharge current, voltage cut-off range, temperature, external pressure, etc., (5) number of cycles at 80% capacity retention, and (6) achieved specific capacity based on cathode materials if coin cells are tested or specific energy in pouch cell cases. Beyond these key parameters, we strongly recommend that electrolyte works (or even all battery works) show at least two replicated cell data for any single cycling condition.

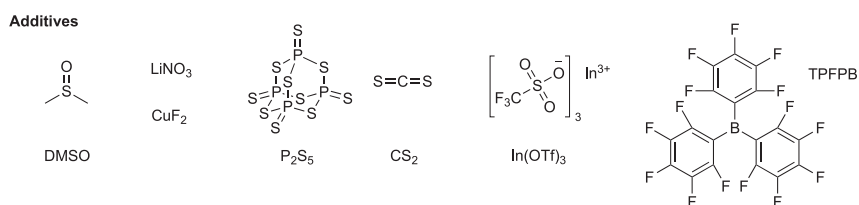
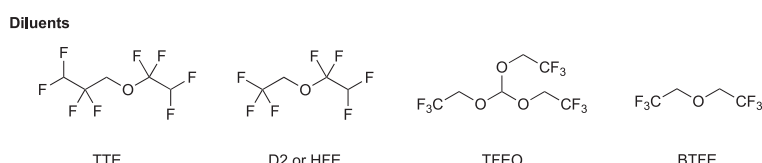
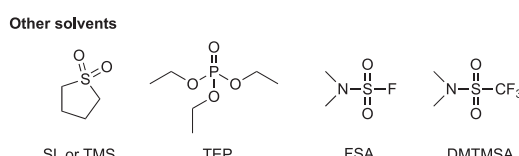
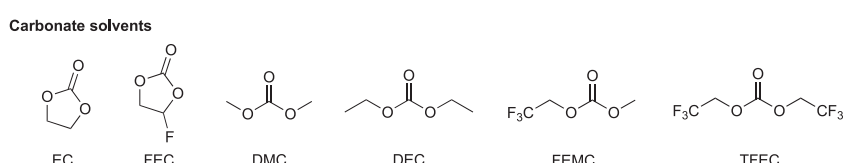
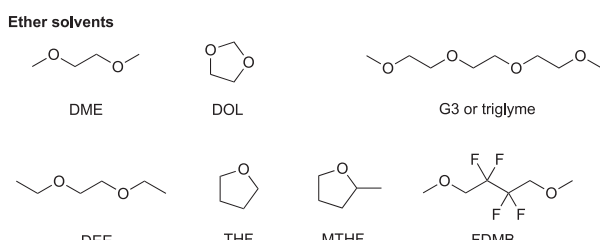
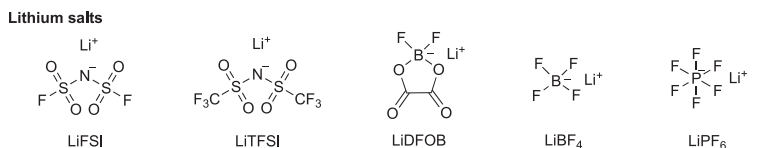
Besides, special recommendations for measuring and reporting CE need to be considered. It is noteworthy at the beginning that the correlation between CE and full-cell cycling performance may not be as tight as we previously expected, because a small excess of Li inventory in the testing cell can yield overestimation of CE.<sup>38</sup> However, the CE of either LMAs or full cells is still an important and direct indicator for Li metal cycling performance, and, therefore, is recommended to be reported following certain protocols. Most previous reports plotted CE with y axis ranging from 0% to 100%, which disabled unambiguous observation of either initial CE activation<sup>35</sup> or its fluctuation. For Li||Cu half cells, three plots are suggested to clearly report Li metal CE: (1) zoomed-in plot starting from the first cycle to the initial tens of cycles, to show how fast Li metal anode can be activated, (2) long-term cycling CE with y axis scale at least from 90% to 100%, to show the efficiency as well as fluctuation over cycles, and (3) modified Aurbach protocol,<sup>38,208</sup> which determines the average Li metal CE. For Li||cathode full cells or Cu||cathode anode-free cells, (1) and (2) can be implemented in the report.

Because the testing protocol will vastly influence the CE results, we, herein, summarize and propose general protocols for standardization:

- (1) Li||Cu half cells: the standard and commonly accepted current density and areal capacity are 0.5 mA/cm<sup>2</sup> and 1 mAh/cm<sup>2</sup>, respectively, which can be the minimum required values for Li||Cu long-term plating/stripping and modified Aurbach protocol.<sup>38,208</sup> Higher values are more desired.
- (2) Li||cathode and Cu||cathode full cells<sup>38</sup>: high-loading (up to 4–5 mAh/cm<sup>2</sup>), high-voltage (>4.2 V) cathodes are desired for maximizing energy density; however, LFP should also be seriously considered due to its low cost and recent prevalence in market. Generally, using a cathode with areal loading >1 mAh/cm<sup>2</sup> in liquid

electrolyte works is highly recommended. Current density of  $>0.5 \text{ mA/cm}^2$  is desired for low-loading ( $<2 \text{ mAh/cm}^2$ ) full cells; while for high-loading ( $4-5 \text{ mAh/cm}^2$ ) ones, slower cycling rate (e.g., C/10 charge C/3 discharge) can be implemented.

## **APPENDIX 1: KEY CHEMICAL STRUCTURES OF LI SALTS, SOLVENTS, ADDITIVES, AND DILUENTS IN TABLE 1 AND 2.**



## ACKNOWLEDGMENTS

The authors acknowledge support from the Assistant Secretary for Energy Efficiency and Renewable Energy, Office of Vehicle Technologies of the U.S. Department of

Energy, under the Battery Materials Research (BMR) program and Battery500 Consortium.

## DECLARATION OF INTERESTS

The authors declare no competing interests.

## REFERENCES

1. Chu, S., Cui, Y., and Liu, N. (2016). The path towards sustainable energy. *Nat. Mater.* 16, 16–22.
2. Lin, D., Liu, Y., and Cui, Y. (2017). Reviving the lithium metal anode for high-energy batteries. *Nat. Nanotechnol.* 12, 194–206.
3. Liu, Y., Zhou, G., Liu, K., and Cui, Y. (2017). Design of complex nanomaterials for energy storage: past success and future opportunity. *Acc. Chem. Res.* 50, 2895–2905.
4. Wu, H., Jia, H., Wang, C., Zhang, J.-G., and Xu, W. (2021). Recent progress in understanding solid electrolyte interphase on lithium metal anodes. *Adv. Energy Mater.* 11, 2003092.
5. Wang, H., Liu, Y., Li, Y., and Cui, Y. (2019). Lithium metal anode materials design: interphase and host. *Electrochem. Energ. Rev.* 2, 509–517.
6. Zhang, J.-G., Xu, W., Xiao, J., Cao, X., and Liu, J. (2020). Lithium metal anodes with nonaqueous electrolytes. *Chem. Rev.* 120, 13312–13348.
7. Yan, K., Lu, Z., Lee, H.-W., Xiong, F., Hsu, P.-C., Li, Y., Zhao, J., Chu, S., and Cui, Y. (2016). Selective deposition and stable encapsulation of lithium through heterogeneous seeded growth. *Nat. Energy* 1, 16010.
8. Wang, H., Lin, D., Xie, J., Liu, Y., Chen, H., Li, Y., Xu, J., Zhou, G., Zhang, Z., Pei, A., et al. (2019). An interconnected channel-like framework as host for lithium metal composite anodes. *Adv. Energy Mater.* 9, 1802720.
9. Lin, D., Liu, Y., Liang, Z., Lee, H.-W., Sun, J., Wang, H., Yan, K., Xie, J., and Cui, Y. (2016). Layered reduced graphene oxide with nanoscale interlayer gaps as a stable host for lithium metal anodes. *Nat. Nanotechnol.* 11, 626–632.
10. Wang, H., Cao, X., Gu, H., Liu, Y., Li, Y., Zhang, Z., Huang, W., Wang, H., Wang, J., Xu, W., et al. (2020). Improving lithium metal composite anodes with seeding and pillarizing effects of silicon nanoparticles. *ACS Nano* 14, 4601–4608.
11. Chen, H., Pei, A., Wan, J., Lin, D., Vilá, R., Wang, H., Mackanic, D., Steinrück, H.-G., Huang, W., Li, Y., et al. (2020). Tortuosity effects in lithium-metal Host Anodes. *Joule* 4, 938–952.
12. Niu, C., Pan, H., Xu, W., Xiao, J., Zhang, J.G., Luo, L., Wang, C., Mei, D., Meng, J., Wang, X., et al. (2019). Self-smoothing anode for achieving high-energy lithium metal batteries under realistic conditions. *Nat. Nanotechnol.* 14, 594–601.
13. Wang, H., Li, Y., Li, Y., Liu, Y., Lin, D., Zhu, C., Chen, G., Yang, A., Yan, K., Chen, H., et al. (2019). Wrinkled graphene cages as Hosts for High-Capacity Li Metal Anodes Shown by Cryogenic Electron Microscopy. *Nano Lett* 19, 1326–1335.
14. Yu, Z., Cui, Y., and Bao, Z. (2020). Design principles of artificial solid electrolyte interphases for lithium-metal anodes. *Cell Rep. Physiol. Sci.* 1, 100119.
15. Yu, Z., Mackanic, D.G., Michaels, W., Lee, M., Pei, A., Feng, D., Zhang, Q., Tsao, Y., Amanchukwu, C.V., Yan, X., et al. (2019). A dynamic, electrolyte-blocking, and single-ion-conductive network for stable lithium-metal anodes. *Joule* 3, 2761–2776.
16. Weng, Y.-T., Liu, H.-W., Pei, A., Shi, F., Wang, H., Lin, C.-Y., Huang, S.-S., Su, L.-Y., Hsu, J.-P., Fang, C.-C., et al. (2019). An ultrathin ionomer interphase for high efficiency lithium anode in carbonate based electrolyte. *Nat. Commun.* 10, 5824.
17. Li, N.-W., Yin, Y.-X., Yang, C.-P., and Guo, Y.-G. (2016). An artificial solid electrolyte interphase layer for stable lithium metal anodes. *Adv. Mater.* 28, 1853–1858.
18. Gao, Y., Rojas, T., Wang, K., Liu, S., Wang, D., Chen, T., Wang, H., Ngo, A.T., and Wang, D. (2020). Low-temperature and high-rate-charging lithium metal batteries enabled by an electrochemically active monolayer-regulated interface. *Nat. Energy* 5, 534–542.
19. Gao, Y., Yan, Z., Gray, J.L., He, X., Wang, D., Chen, T., Huang, Q., Li, Y.C., Wang, H., Kim, S.H., et al. (2019). Polymer-inorganic solid-electrolyte interphase for stable lithium metal batteries under lean electrolyte conditions. *Nat. Mater.* 18, 384–389.
20. Huang, Z., Choudhury, S., Gong, H., Cui, Y., and Bao, Z. (2020). A cation-tethered flowable polymeric interface for enabling stable deposition of metallic lithium. *J. Am. Chem. Soc.* 142, 21393–21403.
21. Kim, M.S., Ryu, J.-H., Deepika, Lim, Y.R., Nah, I.W., Lee, K.-R., Archer, L.A., and Cho, W.I. (2018). Langmuir–Blodgett artificial solid-electrolyte interphases for practical lithium metal batteries. *Nat. Energy* 3, 889–898.
22. Li, J., Cai, Y., Wu, H., Yu, Z., Yan, X., Zhang, Q., Gao, T.Z., Liu, K., Jia, X., and Bao, Z. (2021). Polymers in lithium-ion and lithium metal batteries. *Adv. Energy Mater.* 11, 2003239.
23. Nanda, S., Gupta, A., and Manthiram, A. (2021). Anode-free full cells: a pathway to high-energy density lithium-metal batteries. *Adv. Energy Mater.* 11, 2000804.
24. Fan, X., and Wang, C. (2021). High-voltage liquid electrolytes for Li batteries: progress and perspectives. *Chem. Soc. Rev.* 50, 10486–10566.
25. Hobold, G.M., Lopez, J., Guo, R., Minafra, N., Banerjee, A., Shirley Meng, Y.S., Shao-Horn, Y., and Gallant, B.M. (2021). Moving beyond 99.9% Coulombic efficiency for lithium anodes in liquid electrolytes. *Nat. Energy* 6, 951–960.
26. Flamme, B., Rodriguez Garcia, G., Weil, M., Haddad, M., Phansavath, P., Ratovelomanana-Vidal, V., and Chagnes, A. (2017). Guidelines to design organic electrolytes for lithium-ion batteries: environmental impact, physicochemical and electrochemical properties. *Green Chem* 19, 1828–1849.
27. Yuan, S., Kong, T., Zhang, Y., Dong, P., Zhang, Y., Dong, X., Wang, Y., and Xia, Y. (2021). Advanced electrolyte design for high-energy-density Li-metal batteries under practical conditions. *Angew. Chem. Int. Ed. Engl.* 60, 25624–25638.
28. Peled, E. (1979). The electrochemical behavior of alkali and alkaline earth metals in nonaqueous battery systems—the solid electrolyte interphase model. *J. Electrochem. Soc.* 126, 2047–2051.
29. Koch, V.R., and Young, J.H. (1978). The stability of the secondary lithium electrode in tetrahydrofuran-based electrolytes. *J. Electrochem. Soc.* 125, 1371–1377.
30. Foos, J.S., and McVeigh, J. (1983). Lithium cycling in polymethoxymethane solvents. *J. Electrochem. Soc.* 130, 628–630.
31. Xu, K. (2019). A long journey of lithium: from the big bang to our smartphones. *Energy Environ. Mater.* 2, 229–233.
32. Amanchukwu, C.V., Yu, Z., Kong, X., Qin, J., Cui, Y., and Bao, Z. (2020). A new class of ionically conducting fluorinated ether electrolytes with high electrochemical stability. *J. Am. Chem. Soc.* 142, 7393–7403.
33. Aurbach, D., Daroux, M.L., Faguy, P.W., and Yeager, E. (1987). Identification of surface films formed on lithium in propylene carbonate solutions. *J. Electrochem. Soc.* 134, 1611–1620.
34. Qian, J., Henderson, W.A., Xu, W., Bhattacharya, P., Engelhard, M., Borodin, O., and Zhang, J.G. (2015). High rate and stable cycling of lithium metal anode. *Nat. Commun.* 6, 6362.
35. Yu, Z., Wang, H., Kong, X., Huang, W., Tsao, Y., Mackanic, D.G., Wang, K., Wang, X., Huang, W., Choudhury, S., et al. (2020). Molecular design for electrolyte solvents enabling energy-dense and long-cycling lithium metal batteries. *Nat. Energy* 5, 526–533.

36. Li, W., Yao, H., Yan, K., Zheng, G., Liang, Z., Chiang, Y.M., and Cui, Y. (2015). The synergistic effect of lithium polysulfide and lithium nitrate to prevent lithium dendrite growth. *Nat. Commun.* 6, 7436.
37. Fang, C., Li, J., Zhang, M., Zhang, Y., Yang, F., Lee, J.Z., Lee, M.H., Alvarado, J., Schroeder, M.A., Yang, Y., et al. (2019). Quantifying inactive lithium in lithium metal batteries. *Nature* 572, 511–515.
38. Xiao, J., Li, Q., Bi, Y., Cai, M., Dunn, B., Glossmann, T., Liu, J., Osaka, T., Sugiura, R., Wu, B., et al. (2020). Understanding and applying coulombic efficiency in lithium metal batteries. *Nat. Energy* 5, 561–568.
39. Louli, A.J., Eldesoky, A., Weber, R., Genovese, M., Coon, M., deGooyer, J., Deng, Z., White, R.T., Lee, J., Rodgers, T., et al. (2020). Diagnosing and correcting anode-free cell failure via electrolyte and morphological analysis. *Nat. Energy* 5, 693–702.
40. Kasnatscheew, J., Evertz, M., Streipert, B., Wagner, R., Klöpsch, R., Vortmann, B., Hahn, H., Nowak, S., Amereller, M., Gentschev, A.-C., et al. (2016). The truth about the 1st cycle Coulombic efficiency of LiNi<sub>1/3</sub>Co<sub>1/3</sub>Mn<sub>1/3</sub>O<sub>2</sub> (NCM) cathodes. *Phys. Chem. Chem. Phys.* 18, 3956–3965.
41. Zhou, H., Xin, F., Pei, B., and Whittingham, M.S. (2019). What limits the capacity of layered oxide cathodes in lithium batteries? *ACS Energy Lett.* 4, 1902–1906.
42. Cao, X., Ren, X., Zou, L., Engelhard, M.H., Huang, W., Wang, H., Matthews, B.E., Lee, H., Niu, C., Arey, B.W., et al. (2019). Monolithic solid-electrolyte interphases formed in fluorinated orthoformate-based electrolytes minimize Li depletion and pulverization. *Nat. Energy* 4, 796–805.
43. Chen, J., Li, Q., Pollard, T.P., Fan, X., Borodin, O., and Wang, C. (2020). Electrolyte design for Li metal-free Li batteries. *Mater. Today* 39, 118–126.
44. Niu, C., Lee, H., Chen, S., Li, Q., Du, J., Xu, W., Zhang, J.-G., Whittingham, M.S., Xiao, J., and Liu, J. (2019). High-energy lithium metal pouch cells with limited anode swelling and long stable cycles. *Nat. Energy* 4, 551–559.
45. Duffner, F., Kronemeyer, N., Tübke, J., Leker, J., Winter, M., and Schmuck, R. (2021). Post-lithium-ion battery cell production and its compatibility with lithium-ion cell production infrastructure. *Nat. Energy* 6, 123–134.
46. Qian, J., Adams, B.D., Zheng, J., Xu, W., Henderson, W.A., Wang, J., Bowden, M.E., Xu, S., Hu, J., and Zhang, J.-G. (2016). Anode-free rechargeable lithium metal batteries. *Adv. Funct. Mater.* 26, 7094–7102.
47. Suo, L., Xue, W., Gobet, M., Greenbaum, S.G., Wang, C., Chen, Y., Yang, W., Li, Y., and Li, J. (2018). Fluorine-donating electrolytes enable highly reversible 5-V-class Li metal batteries. *Proc. Natl. Acad. Sci. USA* 115, 1156–1161.
48. Beyene, T.T., Jote, B.A., Wondimkun, Z.T., Olbassa, B.W., Huang, C.-J., Thirumalraj, B., Wang, C.-H., Su, W.-N., Dai, H., and Hwang, B.-J. (2019). Effects of concentrated salt and resting protocol on solid electrolyte interface formation for improved cycle stability of anode-free lithium metal batteries. *ACS Appl. Mater. Interfaces* 11, 31962–31971.
49. Hagos, T.T., Thirumalraj, B., Huang, C.-J., Abhra, L.H., Hagos, T.M., Berhe, G.B., Bezabih, H.K., Cherng, J., Chiu, S.-F., Su, W.-N., and Hwang, B.-J. (2019). Locally concentrated LiPF<sub>6</sub> in a carbonate-based electrolyte with fluoroethylene carbonate as a diluent for anode-free lithium metal batteries. *ACS Appl. Mater. Interfaces* 11, 9955–9963.
50. Ren, X., Zou, L., Cao, X., Engelhard, M.H., Liu, W., Burton, S.D., Lee, H., Niu, C., Matthews, B.E., Zhu, Z., et al. (2019). Enabling high-voltage lithium-metal batteries under practical conditions. *Joule* 3, 1662–1676.
51. Wang, H., Yu, Z., Kong, X., Huang, W., Zhang, Z., Mackanic, D.G., Huang, X., Qin, J., Bao, Z., and Cui, Y. (2021). Dual-solvent Li-ion solvation enables high-performance Li-metal batteries. *Adv. Mater.* 33, e2008619.
52. Fan, X., Chen, L., Borodin, O., Ji, X., Chen, J., Hou, S., Deng, T., Zheng, J., Yang, C., Liou, S.-C., et al. (2018). Non-flammable electrolyte enables Li-metal batteries with aggressive cathode chemistries. *Nat. Nanotechnol.* 13, 715–722.
53. Xue, W., Shi, Z., Huang, M., Feng, S., Wang, C., Wang, F., Lopez, J., Qiao, B., Xu, G., Zhang, W., et al. (2020). FSI-inspired solvent and “full fluorosulfonyl” electrolyte for 4 V class lithium-metal batteries. *Energy Environ. Sci.* 13, 212–220.
54. Qiu, F., Li, X., Deng, H., Wang, D., Mu, X., He, P., and Zhou, H. (2019). A concentrated ternary-salts electrolyte for high reversible Li metal battery with slight excess Li. *Adv. Energy Mater.* 9, 1803372.
55. Weber, R., Genovese, M., Louli, A.J., Hames, S., Martin, C., Hill, I.G., and Dahn, J.R. (2019). Long cycle life and dendrite-free lithium morphology in anode-free lithium pouch cells enabled by a dual-salt liquid electrolyte. *Nat. Energy* 4, 683–689.
56. Genovese, M., Louli, A.J., Weber, R., Martin, C., Taskovic, T., and Dahn, J.R. (2019). Hot formation for improved low temperature cycling of anode-free lithium metal batteries. *J. Electrochem. Soc.* 166, A3342–A3347.
57. Louli, A.J., Genovese, M., Weber, R., Hames, S.G., Logan, E.R., and Dahn, J.R. (2019). Exploring the impact of mechanical pressure on the performance of anode-free lithium metal cells. *J. Electrochem. Soc.* 166, A1291–A1299.
58. Zhang, W., Shen, Z., Li, S., Fan, L., Wang, X., Chen, F., Zang, X., Wu, T., Ma, F., and Lu, Y. (2020). Engineering wavy-nanostructured anode interphases with fast ion transfer kinetics: toward practical Li-metal full batteries. *Adv. Funct. Mater.* 30, 2003800.
59. Qiao, Y., Yang, H., Chang, Z., Deng, H., Li, X., and Zhou, H. (2021). A high-energy-density and long-life initial-anode-free lithium battery enabled by a Li<sub>2</sub>O sacrificial agent. *Nat. Energy* 6, 653–662.
60. Fan, X., Chen, L., Ji, X., Deng, T., Hou, S., Chen, J., Zheng, J., Wang, F., Jiang, J., Xu, K., and Wang, C. (2018). Highly fluorinated interphases enable high-voltage Li-metal batteries. *Chem* 4, 174–185.
61. Maeyoshi, Y., Ding, D., Kubota, M., Ueda, H., Abe, K., Kanamura, K., and Abe, H. (2019). Long-term stable lithium metal anode in highly concentrated sulfolane-based electrolytes with ultrafine porous polyimide separator. *ACS Appl. Mater. Interfaces* 11, 25833–25843.
62. Chen, Y., Yu, Z., Rudnicki, P., Gong, H., Huang, Z., Kim, S.C., Lai, J.-C., Kong, X., Qin, J., Cui, Y., and Bao, Z. (2021). Steric effect tuned ion solvation enabling stable cycling of high-voltage lithium metal battery. *J. Am. Chem. Soc.* 143, 18703–18713.
63. Chen, S., Zheng, J., Mei, D., Han, K.S., Engelhard, M.H., Zhao, W., Xu, W., Liu, J., and Zhang, J.-G. (2018). High-voltage lithium-metal batteries enabled by localized high-concentration electrolytes. *Adv. Mater.* 30, e1706102.
64. Chen, S., Zheng, J., Yu, L., Ren, X., Engelhard, M.H., Niu, C., Lee, H., Xu, W., Xiao, J., Liu, J., and Zhang, J.-G. (2018). High-efficiency lithium metal batteries with fire-retardant electrolytes. *Joule* 2, 1548–1558.
65. Yu, L., Chen, S., Lee, H., Zhang, L., Engelhard, M.H., Li, Q., Jiao, S., Liu, J., Xu, W., and Zhang, J.-G. (2018). A localized high-concentration electrolyte with optimized solvents and lithium difluoro(oxalate)borate additive for stable lithium metal batteries. *ACS Energy Lett.* 3, 2059–2067.
66. Ren, X., Chen, S., Lee, H., Mei, D., Engelhard, M.H., Burton, S.D., Zhao, W., Zheng, J., Li, Q., Ding, M.S., et al. (2018). Localized high-concentration sulfone electrolytes for high-efficiency lithium-metal batteries. *Chem* 4, 1877–1892.
67. Xue, W., Huang, M., Li, Y., Zhu, Y.G., Gao, R., Xiao, X., Zhang, W., Li, S., Xu, G., Yu, Y., et al. (2021). Ultra-high-voltage Ni-rich layered cathodes in practical Li metal batteries enabled by a sulfonamide-based electrolyte. *Nat. Energy* 6, 495–505.
68. Jiao, S., Ren, X., Cao, R., Engelhard, M.H., Liu, Y., Hu, D., Mei, D., Zheng, J., Zhao, W., Li, Q., et al. (2018). Stable cycling of high-voltage lithium metal batteries in ether electrolytes. *Nat. Energy* 3, 739–746.
69. Liu, Y., Lin, D., Li, Y., Chen, G., Pei, A., Nix, O., Li, Y., and Cui, Y. (2018). Solubility-mediated sustained release enabling nitrate additive in carbonate electrolytes for stable lithium metal anode. *Nat. Commun.* 9, 3656.
70. Zhang, X.-Q., Chen, X., Cheng, X.-B., Li, B.-Q., Shen, X., Yan, C., Huang, J.-Q., and Zhang, Q. (2018). Highly stable lithium metal batteries enabled by regulating the solvation of lithium ions in nonaqueous electrolytes. *Angew. Chem. Int. Ed. Engl.* 57, 5301–5305.
71. Yan, C., Li, H.-R., Chen, X., Zhang, X.-Q., Cheng, X.-B., Xu, R., Huang, J.-Q., and Zhang, Q. (2019). Regulating the inner helmholtz plane for stable solid electrolyte interphase on lithium metal anodes. *J. Am. Chem. Soc.* 141, 9422–9429.
72. Li, S., Zhang, W., Wu, Q., Fan, L., Wang, X., Wang, X., Shen, Z., He, Y., and Lu, Y. (2020). Synergistic dual-additive electrolyte enables practical lithium-metal batteries. *Angew. Chem. Int. Ed. Engl.* 59, 14935–14941.

73. Liu, S., Ji, X., Piao, N., Chen, J., Eidson, N., Xu, J., Wang, P., Chen, L., Zhang, J., Deng, T., et al. (2021). An inorganic-rich solid electrolyte interphase for advanced lithium-metal batteries in carbonate electrolytes. *Angew. Chem. Int. Ed. Engl.* 60, 3661–3671.
74. Lee, S.H., Hwang, J.-Y., Ming, J., Kim, H., Jung, H.-G., and Sun, Y.-K. (2021). Long-lasting solid electrolyte interphase for stable Li-metal batteries. *ACS Energy Lett* 6, 2153–2161.
75. Yamada, Y., and Yamada, A. (2015). Review—superconcentrated electrolytes for lithium batteries. *J. Electrochem. Soc.* 162, A2406–A2423.
76. Borodin, O., Self, J., Persson, K.A., Wang, C., and Xu, K. (2020). Uncharted waters: superconcentrated electrolytes. *Joule* 4, 69–100.
77. McKinnon, W.R., and Dahn, J.R. (1985). How to reduce the cointercalation of propylene carbonate in  $\text{Li}_x\text{ZrS}_2$  and other layered compounds. *J. Electrochem. Soc.* 132, 364–366.
78. Jeong, S.-K., Inaba, M., Iriyama, Y., Abe, T., and Ogumi, Z. (2003). Electrochemical intercalation of lithium ion within graphite from propylene carbonate solutions. *Electrochim. Solid-State Lett.* 6, A13.
79. Jeong, S.-K., Inaba, M., Iriyama, Y., Abe, T., and Ogumi, Z. (2008). Interfacial reactions between graphite electrodes and propylene carbonate-based solutions: electrolyte-concentration dependence of electrochemical lithium intercalation reaction. *J. Power Sources* 175, 540–546.
80. Yamada, Y., Takazawa, Y., Miyazaki, K., and Abe, T. (2010). Electrochemical lithium intercalation into graphite in dimethyl sulfoxide-based electrolytes: effect of solvation structure of lithium ion. *J. Phys. Chem. C* 114, 11680–11685.
81. Yamada, Y., Furukawa, K., Sodeyama, K., Kikuchi, K., Yaegashi, M., Tateyama, Y., and Yamada, A. (2014). Unusual stability of acetonitrile-based superconcentrated electrolytes for fast-charging lithium-ion batteries. *J. Am. Chem. Soc.* 136, 5039–5046.
82. Suo, L., Borodin, O., Gao, T., Olguin, M., Ho, J., Fan, X., Luo, C., Wang, C., and Xu, K. (2015). “Water-in-salt” electrolyte enables high-voltage aqueous lithium-ion chemistries. *Science* 350, 938–943.
83. Jeong, S.-K., Seo, H.-Y., Kim, D.-H., Han, H.-K., Kim, J.-G., Lee, Y.B., Iriyama, Y., Abe, T., and Ogumi, Z. (2008). Suppression of dendritic lithium formation by using concentrated electrolyte solutions. *Electrochim. Commun.* 10, 635–638.
84. Ren, X., Zou, L., Jiao, S., Mei, D., Engelhard, M.H., Li, Q., Lee, H., Niu, C., Adams, B.D., Wang, C., et al. (2019). High-concentration ether electrolytes for stable high-voltage lithium metal batteries. *ACS Energy Lett* 4, 896–902.
85. Zeng, Z., Murugesan, V., Han, K.S., Jiang, X., Cao, Y., Xiao, L., Ai, X., Yang, H., Zhang, J.-G., Sushko, M.L., and Liu, J. (2018). Non-flammable electrolytes with high salt-to-solvent ratios for Li-ion and Li-metal batteries. *Nat. Energy* 3, 674–681.
86. Dokko, K., Tachikawa, N., Yamauchi, K., Tsuchiya, M., Yamazaki, A., Takashima, E., Park, J.-W., Ueno, K., Seki, S., Serizawa, N., and Watanabe, M. (2013). Solvate ionic liquid electrolyte for Li-S batteries. *J. Electrochem. Soc.* 160, A1304–A1310.
87. Moon, H., Mandai, T., Tataro, R., Ueno, K., Yamazaki, A., Yoshida, K., Seki, S., Dokko, K., and Watanabe, M. (2015). Solvent activity in electrolyte solutions controls electrochemical reactions in Li-Ion and Li-sulfur batteries. *J. Phys. Chem. C* 119, 3957–3970.
88. Ueno, K., Murai, J., Ikeda, K., Suzuki, S., Tsuchiya, M., Tataro, R., Mandai, T., Umebayashi, Y., Dokko, K., and Watanabe, M. (2016). Li+ solvation and ionic transport in lithium solvate ionic liquids diluted by molecular solvents. *J. Phys. Chem. C* 120, 15792–15802.
89. Doi, T., Shimizu, Y., Hashinokuchi, M., and Inaba, M. (2017). Dilution of highly concentrated LiBF4/propylene carbonate electrolyte solution with fluoroalkyl ethers for 5-V  $\text{LiNi}0.5\text{Mn}1.5\text{O}_4$  positive electrodes. *J. Electrochim. Soc.* 164, A6412–A6416.
90. Fan, X., Ji, X., Chen, L., Chen, J., Deng, T., Han, F., Yue, J., Piao, N., Wang, R., Zhou, X., et al. (2019). All-temperature batteries enabled by fluorinated electrolytes with non-polar solvents. *Nat. Energy* 4, 882–890.
91. Xu, R., Ding, J.-F., Ma, X.-X., Yan, C., Yao, Y.-X., and Huang, J.-Q. (2021). Designing and demystifying the lithium metal interface toward highly reversible batteries. *Adv. Mater.* e2105962
92. Hu, M., Wei, J., Xing, L., and Zhou, Z. (2012). Effect of lithium difluoro(oxalate)borate (LiDFOB) additive on the performance of high-voltage lithium-ion batteries. *J. Appl. Electrochim.* 42, 291–296.
93. Yan, C., Yao, Y.-X., Chen, X., Cheng, X.-B., Zhang, X.-Q., Huang, J.-Q., and Zhang, Q. (2018). Lithium nitrate solvation chemistry in carbonate electrolyte sustains high-voltage lithium metal batteries. *Angew. Chem. Int. Ed. Engl.* 57, 14055–14059.
94. Miao, R., Yang, J., Feng, X., Jia, H., Wang, J., and Nuli, Y. (2014). Novel dual-salts electrolyte solution for dendrite-free lithium-metal based rechargeable batteries with high cycle reversibility. *J. Power Sources* 271, 291–297.
95. Schedlbauer, T., Krüger, S., Schmitz, R., Schmitz, R.W., Schreiner, C., Gores, H.J., Passerini, S., and Winter, M. (2013). Lithium difluoro(oxalato)borate: a promising salt for lithium metal based secondary batteries? *Electrochim. Acta* 92, 102–107.
96. Jurng, S., Brown, Z.L., Kim, J., and Lucht, B.L. (2018). Effect of electrolyte on the nanostructure of the solid electrolyte interphase (SEI) and performance of lithium metal anodes. *Energy Environ. Sci.* 11, 2600–2608.
97. Brown, Z.L., and Lucht, B.L. (2019). Synergistic performance of lithium difluoro(oxalato) borate and fluoroethylene carbonate in carbonate electrolytes for lithium metal anodes. *J. Electrochim. Soc.* 166, A5117–A5121.
98. Xu, K. (2004). Nonaqueous liquid electrolytes for lithium-based rechargeable batteries. *Chem. Rev.* 104, 4303–4417.
99. Xu, K. (2014). Electrolytes and interphases in Li-ion batteries and beyond. *Chem. Rev.* 114, 11503–11618.
100. Zhang, H., Eshetu, G.G., Judez, X., Li, C., Rodriguez-Martinez, L.M., and Armand, M. (2018). Electrolyte additives for lithium metal anodes and rechargeable lithium metal batteries: progress and perspectives. *Angew. Chem. Int. Ed. Engl.* 57, 15002–15027.
101. Abraham, K.M., Foos, J.S., and Goldman, J.L. (1984). Long cycle-life secondary lithium cells utilizing tetrahydrofuran. *J. Electrochim. Soc.* 131, 2197–2199.
102. Aurbach, D., Gofer, Y., Ben-Zion, M., and Aped, P. (1992). The behaviour of lithium electrodes in propylene and ethylene carbonate: Te major factors that influence Li cycling efficiency. *J. Electroanal. Chem.* 339, 451–471.
103. Aurbach, D., and Zaban, A. (1994). Impedance spectroscopy of nonactive metal electrodes at low potentials in propylene carbonate solutions: a comparison to studies of Li electrodes. *J. Electrochim. Soc.* 141, 1808–1819.
104. Matsuda, Y. (1993). Behavior of lithium/electrolyte interface in organic solutions. *J. Power Sources* 43, 1–7.
105. Yoon, S., Lee, J., Kim, S.-O., and Sohn, H.-J. (2008). Enhanced cyclability and surface characteristics of lithium batteries by Li-Mg co-deposition and addition of HF acid in electrolyte. *Electrochim. Acta* 53, 2501–2506.
106. Vega, J.A., Zhou, J., and Kohl, P.A. (2009). Electrochemical comparison and deposition of lithium and potassium from phosphonium- and ammonium-TFSI ionic liquids. *J. Electrochim. Soc.* 156, A253.
107. Stark, J.K., Ding, Y., and Kohl, P.A. (2011). Dendrite-free electrodeposition and reoxidation of lithium-sodium alloy for metal-anode battery. *J. Electrochim. Soc.* 158, A1100.
108. Ding, F., Xu, W., Graff, G.L., Zhang, J., Sushko, M.L., Chen, X., Shao, Y., Engelhard, M.H., Nie, Z., Xiao, J., et al. (2013). Dendrite-free lithium deposition via self-healing electrostatic shield mechanism. *J. Am. Chem. Soc.* 135, 4450–4456.
109. Qian, J., Xu, W., Bhattacharya, P., Engelhard, M., Henderson, W.A., Zhang, Y., and Zhang, J.-G. (2015). Dendrite-free Li deposition using trace-amounts of water as an electrolyte additive. *Nano Energy* 15, 135–144.
110. Ren, X., Zhang, Y., Engelhard, M.H., Li, Q., Zhang, J.-G., and Xu, W. (2018). Guided lithium metal deposition and improved lithium coulombic efficiency through synergistic effects of LiAsF6 and cyclic carbonate additives. *ACS Energy Lett* 3, 14–19.
111. Li, X., Zheng, J., Ren, X., Engelhard, M.H., Zhao, W., Li, Q., Zhang, J.-G., and Xu, W. (2018). Dendrite-free and performance-enhanced lithium metal batteries through optimizing solvent compositions and adding

- combinational additives. *Adv. Energy Mater.* 8, 1703022.
112. Zhang, X.-Q., Cheng, X.-B., Chen, X., Yan, C., and Zhang, Q. (2017). Fluoroethylene carbonate additives to render uniform Li deposits in lithium metal batteries. *Adv. Funct. Mater.* 27, 1605989.
113. Wang, J., Huang, W., Pei, A., Li, Y., Shi, F., Yu, X., and Cui, Y. (2019). Improving cyclability of Li metal batteries at elevated temperatures and its origin revealed by cryo-electron microscopy. *Nat. Energy* 4, 664–670.
114. Shi, Q., Zhong, Y., Wu, M., Wang, H., and Wang, H. (2018). High-capacity rechargeable batteries based on deeply cyclable lithium metal anodes. *Proc. Natl. Acad. Sci. USA* 115, 5676–5680.
115. Oyakhire, S.T., Huang, W., Wang, H., Boyle, D.T., Schneider, J.R., de Paula, C., Wu, Y., Cui, Y., and Bent, S.F. (2020). Revealing and elucidating ALD-derived control of lithium plating microstructure. *Adv. Energy Mater.* 10, 2002736.
116. Lu, Y., Tu, Z., and Archer, L.A. (2014). Stable lithium electrodeposition in liquid and nanoporous solid electrolytes. *Nat. Mater.* 13, 961–969.
117. Cheng, X.B., Zhao, M.Q., Chen, C., Pentecost, A., Maleski, K., Mathis, T., Zhang, X.Q., Zhang, Q., Jiang, J., and Gogotsi, Y. (2017). Nanodiamonds suppress the growth of lithium dendrites. *Nat. Commun.* 8, 336.
118. Li, Y., Huang, W., Li, Y., Pei, A., Boyle, D.T., and Cui, Y. (2018). Correlating structure and function of battery interphases at atomic resolution using cryoelectron microscopy. *Joule* 2, 2167–2177.
119. Li, Y., Li, Y., Pei, A., Yan, K., Sun, Y., Wu, C.L., Joubert, L.M., Chin, R., Koh, A.L., Yu, Y., et al. (2017). Atomic structure of sensitive battery materials and interfaces revealed by cryo-electron microscopy. *Science* 358, 506–510.
120. Yang, Y., Davies, D.M., Yin, Y., Borodin, O., Lee, J.Z., Fang, C., Olgun, M., Zhang, Y., Sablina, E.S., Wang, X., et al. (2019). High-efficiency lithium-metal anode enabled by liquefied gas electrolytes. *Joule* 3, 1986–2000.
121. Rustomji, C.S., Yang, Y., Kim, T.K., Mac, J., Kim, Y.J., Caldwell, E., Chung, H., and Meng, Y.S. (2017). Liquefied gas electrolytes for electrochemical energy storage devices. *Science* 356, eaal4263.
122. Yang, Y., Yin, Y., Davies, D.M., Zhang, M., Mayer, M., Zhang, Y., Sablina, E.S., Wang, S., Lee, J.Z., Borodin, O., et al. (2020). Liquefied gas electrolytes for wide-temperature lithium metal batteries. *Energy Environ. Sci.* 13, 2209–2219.
123. Pei, A., Zheng, G., Shi, F., Li, Y., and Cui, Y. (2017). Nanoscale nucleation and growth of electrodeposited lithium metal. *Nano Lett* 17, 1132–1139.
124. Wang, X., Zhang, M., Alvarado, J., Wang, S., Sina, M., Lu, B., Bouwer, J., Xu, W., Xiao, J., Zhang, J.-G., et al. (2017). New insights on the structure of electrochemically deposited lithium metal and its solid electrolyte interphases via cryogenic TEM. *Nano Lett* 17, 7606–7612.
125. Zachman, M.J., Tu, Z., Choudhury, S., Archer, L.A., and Kourkoutis, L.F. (2018). Cryo-STEM mapping of solid–liquid interfaces and dendrites in lithium–metal batteries. *Nature* 560, 345–349.
126. Peled, E., Golodnitsky, D., and Ardel, G. (1997). Advanced model for solid electrolyte interphase electrodes in liquid and polymer electrolytes. *J. Electrochem. Soc.* 144, L208–L210.
127. Aurbach, D., Ein-Ely, Y., and Zaban, A. (1994). The surface chemistry of lithium electrodes in alkyl carbonate solutions. *J. Electrochem. Soc.* 141, L1–L3.
128. Liu, S., Ji, X., Yue, J., Hou, S., Wang, P., Cui, C., Chen, J., Shao, B., Li, J., Han, F., et al. (2020). High interfacial-energy interphase promoting safe lithium metal batteries. *J. Am. Chem. Soc.* 142, 2438–2447.
129. Kim, S.C., Kong, X., Vilá, R.A., Huang, W., Chen, Y., Boyle, D.T., Yu, Z., Wang, H., Bao, Z., Qin, J., and Cui, Y. (2021). Potentiometric measurement to probe solvation energy and its correlation to lithium battery cyclability. *J. Am. Chem. Soc.* 143, 10301–10308.
130. Wang, H., Kim, S.C., Rojas, T., Zhu, Y., Li, Y., Ma, L., Xu, K., Ngo, A.T., and Cui, Y. (2021). Correlating Li-ion solvation structures and electrode potential temperature coefficients. *J. Am. Chem. Soc.* 143, 2264–2271.
131. Huang, W., Wang, H., Boyle, D.T., Li, Y., and Cui, Y. (2020). Resolving nanoscopic and mesoscopic heterogeneity of fluorinated species in battery solid-electrolyte interphases by cryogenic electron microscopy. *ACS Energy Lett* 5, 1128–1135.
132. Wang, H., Huang, W., Yu, Z., Huang, W., Xu, R., Zhang, Z., Bao, Z., and Cui, Y. (2021). Efficient lithium metal cycling over a Wide Range of pressures from an anion-derived solid-electrolyte interphase framework. *ACS Energy Lett* 6, 816–825.
133. Li, G., and Monroe, C.W. (2020). Multiscale lithium-battery modeling from materials to cells. *Annu. Rev. Chem. Biomol. Eng.* 11, 277–310.
134. Li, T., and Balbuena, P.B. (2000). Theoretical studies of the reduction of ethylene carbonate. *Chem. Phys. Lett.* 317, 421–429.
135. Kim, D., Guk, H., Choi, S.-H., and Chung, D.H. (2017). Benchmarking of computational approaches for fast screening of lithium ion battery electrolyte solvents. *Chem. Phys. Lett.* 681, 64–68.
136. Borodin, O., Olgun, M., Spear, C.E., Leiter, K.W., and Knap, J. (2015). Towards high throughput screening of electrochemical stability of battery electrolytes. *Nanotechnology* 26, 354003.
137. Cheng, L., Assary, R.S., Qu, X., Jain, A., Ong, S.P., Rajput, N.N., Persson, K., and Curtiss, L.A. (2015). Accelerating electrolyte discovery for energy storage with high-throughput screening. *J. Phys. Chem. Lett.* 6, 283–291.
138. Husch, T., and Korth, M. (2015). How to estimate solid-electrolyte-interphase features when screening electrolyte materials. *Phys. Chem. Chem. Phys.* 17, 22799–22808.
139. Qu, X., Jain, A., Rajput, N.N., Cheng, L., Zhang, Y., Ong, S.P., Brafman, M., Maginn, E., Curtiss, L.A., and Persson, K.A. (2015). The Electrolyte Genome project: a big data approach in battery materials discovery. *Comput. Mater. Sci.* 103, 56–67.
140. Endo, E., Ata, M., Tanaka, K., and Sekai, K. (1988). Electron spin resonance study of the electrochemical reduction of electrolyte solutions for lithium secondary batteries. *J. Electrochem. Soc.* 145, 3757–3764.
141. Hou, T., Yang, G., Rajput, N.N., Self, J., Park, S.-W., Nanda, J., and Persson, K.A. (2019). The influence of FEC on the solvation structure and reduction reaction of LiPF<sub>6</sub>/EC electrolytes and its implication for solid electrolyte interphase formation. *Nano Energy* 64, 103881.
142. Hanke, F., Modrow, N., Akkermans, R.L.C., Korotkin, I., Mocanu, F.C., Neufeld, V.A., and Veit, M. (2020). Multi-scale electrolyte transport simulations for lithium ion batteries. *J. Electrochem. Soc.* 167, 013522.
143. You, X., Chaudhari, M.I., Rempe, S.B., and Pratt, L.R. (2016). Dielectric relaxation of ethylene carbonate and propylene carbonate from molecular dynamics simulations. *J. Phys. Chem. B* 120, 1849–1853.
144. Ushirogata, K., Sodeyama, K., Okuno, Y., and Tateyama, Y. (2013). Additive effect on reductive decomposition and binding of carbonate-based solvent toward solid electrolyte interphase formation in lithium-ion battery. *J. Am. Chem. Soc.* 135, 11967–11974.
145. Yu, J., Balbuena, P.B., Budzien, J., and Leung, K. (2011). Hybrid DFT functional-based static and molecular dynamics studies of excess electron in liquid ethylene carbonate. *J. Electrochem. Soc.* 158, A400.
146. Islam, M.M., and van Duin, A.C.T. (2016). Reductive decomposition reactions of ethylene carbonate by explicit electron transfer from lithium: an eReaxFF molecular dynamics study. *J. Phys. Chem. C* 120, 27128–27134.
147. Kim, S.-P., van Duin, A.C.T., and Shenoy, V.B. (2011). Effect of electrolytes on the structure and evolution of the solid electrolyte interphase (SEI) in Li-ion batteries: a molecular dynamics study. *J. Power Sources* 196, 8590–8597.
148. Franco, A.A., Rucci, A., Brandell, D., Frayret, C., Gaberscik, M., Jankowski, P., and Johansson, P. (2019). Boosting rechargeable batteries R&D by multiscale modeling: myth or reality? *Chem. Rev.* 119, 4569–4627.
149. Qiao, B., Mohapatra, S., Lopez, J., Leverick, G.M., Tatar, R., Shibuya, Y., Jiang, Y., France-Lanord, A., Grossman, J.C., Gómez-Bombarelli, R., et al. (2020). Quantitative mapping of molecular substituents to macroscopic properties enables predictive design of oligoethylene glycol-based lithium electrolytes. *ACS Cent. Sci.* 6, 1115–1128.
150. Lombardo, T., Duquesnoy, M., El-Bousyid, H., Áren, F., Gallo-Bueno, A., Jørgensen, P.B., Bhowmik, A., Demortière, A., Ayerbe, E., Alcaide, F., et al. (2021). Artificial intelligence applied to battery research: hype or reality?

- Chem. Rev. <https://doi.org/10.1021/acs.chemrev.1c00108>.
151. Chen, X., Liu, X., Shen, X., and Zhang, Q. (2021). Applying machine learning to rechargeable batteries: from the microscale to the macroscale. *Angew. Chem. Int. Ed. Engl.* 60, 24354–24366.
  152. Sendek, A.D., Cubuk, E.D., Antoniuk, E.R., Cheon, G., Cui, Y., and Reed, E.J. (2019). Machine learning-assisted discovery of solid Li-ion conducting materials. *Chem. Mater.* 31, 342–352.
  153. Severson, K.A., Attia, P.M., Jin, N., Perkins, N., Jiang, B., Yang, Z., Chen, M.H., Aykol, M., Herring, P.K., Fragedakis, D., et al. (2019). Data-driven prediction of battery cycle life before capacity degradation. *Nat. Energy* 4, 383–391.
  154. Attia, P.M., Grover, A., Jin, N., Severson, K.A., Markov, T.M., Liao, Y.H., Chen, M.H., Cheong, B., Perkins, N., Yang, Z., et al. (2020). Closed-loop optimization of fast-charging protocols for batteries with machine learning. *Nature* 578, 397–402.
  155. Jie, Y., Ren, X., Cao, R., Cai, W., and Jiao, S. (2020). Advanced liquid electrolytes for rechargeable Li metal batteries. *Adv. Funct. Mater.* 30, 1910777.
  156. R.T. Jow, K. Xu, O. Borodin, and M. Ue, eds. (2014). *Electrolytes for Lithium and Lithium-Ion Batteries* (Springer).
  157. Younesi, R., Veith, G.M., Johansson, P., Edström, K., and Vegge, T. (2015). Lithium salts for advanced lithium batteries: Li–metal, Li–O<sub>2</sub>, and Li–S. *Energy Environ. Sci.* 8, 1905–1922.
  158. Armand, M., Johansson, P., Bukowska, M., Szczęciński, P., Niedzicki, L., Marcinek, M., Dranka, M., Zachara, J., Żukowska, G., Marczewski, M., et al. (2020). Review—development of Hückel type anions: from molecular modeling to industrial commercialization. A success story. *J. Electrochem. Soc.* 167, 070562.
  159. Hall, D.S., Hynes, T., Aiken, C.P., and Dahn, J.R. (2020). Synthesis and evaluation of Difluorophosphate salt electrolyte additives for lithium-ion batteries. *J. Electrochem. Soc.* 167, 100538.
  160. Zheng, H., Xiang, H., Jiang, F., Liu, Y., Sun, Y., Liang, X., Feng, Y., and Yu, Y. (2020). Lithium difluorophosphate-based dual-salt low concentration electrolytes for lithium metal batteries. *Adv. Energy Mater.* 10, 2001440.
  161. Gnanaraj, J.S., Zinigrad, E., Asraf, L., Sprecher, M., Gottlieb, H.E., Geissler, W., Schmidt, M., and Aurbach, D. (2003). On the use of LiPF<sub>3</sub>(CF<sub>2</sub>CF<sub>3</sub>)<sub>3</sub> (LiFAP) solutions for Li-ion batteries. *Electrochemical and thermal studies. Electrochim. Commun.* 5, 946–951.
  162. Qin, Y., Chen, Z., Liu, J., and Amine, K. (2010). Lithium tetrafluoro oxalato phosphate as electrolyte additive for lithium-ion cells. *Electrochim. Solid-State Lett.* 13, A11.
  163. Huang, M., Feng, S., Zhang, W., Lopez, J., Qiao, B., Tatara, R., Giordano, L., Shao-Horn, Y., and Johnson, J.A. (2019). Design of S-substituted fluorinated aryl sulfonamide-tagged (S-FAST) anions to enable new solvate ionic liquids for battery applications. *Chem. Mater.* 31, 7558–7564.
  164. Tong, B., Wang, P., Ma, Q., Wan, H., Zhang, H., Huang, X., Armand, M., Feng, W., Nie, J., and Zhou, Z. (2020). Lithium fluorinated sulfonimide-based solid polymer electrolytes for Li || LiFePO<sub>4</sub> cell: the impact of anionic structure. *Solid State Ionics* 358, 115519.
  165. Zhang, H., Oteo, U., Zhu, H., Judez, X., Martínez-Ibáñez, M., Aldalur, I., Sanchez-Diez, E., Li, C., Carrasco, J., Forsyth, M., and Armand, M. (2019). Enhanced lithium-ion conductivity of polymer electrolytes by selective introduction of hydrogen into the anion. *Angew. Chem. Int. Ed. Engl.* 58, 7829–7834.
  166. Zhang, W., Feng, S., Huang, M., Qiao, B., Shigenobu, K., Giordano, L., Lopez, J., Tatara, R., Ueno, K., Dokko, K., et al. (2021). Molecularly Tunable polyanions for Single-Ion Conductors and poly(solvate ionic liquids). *Chem. Mater.* 33, 524–534.
  167. Xiao, Y., Han, B., Zeng, Y., Chi, S.-S., Zeng, X., Zheng, Z., Xu, K., and Deng, Y. (2020). New lithium salt forms interphases suppressing both Li dendrite and polysulfide shuttling. *Adv. Energy Mater.* 10, 1903937.
  168. Shangguan, X., Xu, G., Cui, Z., Wang, Q., Du, X., Chen, K., Huang, S., Jia, G., Li, F., Wang, X., et al. (2019). Additive-assisted novel dual-salt electrolyte addresses wide temperature operation of lithium–metal batteries. *Small* 15, e1900269.
  169. Qiao, L., Cui, Z., Chen, B., Xu, G., Zhang, Z., Ma, J., Du, H., Liu, X., Huang, S., Tang, K., et al. (2018). A promising bulky anion based lithium borate salt for lithium metal batteries. *Chem. Sci.* 9, 3451–3458.
  170. Chae, O.B., Adiraju, V.A.K., and Lucht, B.L. (2021). Lithium cyano Tris(2,2,2-trifluoroethyl) borate as a multifunctional electrolyte additive for high-performance lithium metal batteries. *ACS Energy Lett.* 6, 3851–3857.
  171. Wang, Z., Qi, F., Yin, L., Shi, Y., Sun, C., An, B., Cheng, H.-M., and Li, F. (2020). An anion-tuned solid electrolyte interphase with fast ion transfer kinetics for stable lithium anodes. *Adv. Energy Mater.* 10, 1903843.
  172. Ramar, V., Pszolla, C., Rapp, M., Borck, M., and Zinck, L. (2020). Non-flammable inorganic liquid electrolyte lithium-ion batteries. *J. Electrochem. Soc.* 167, 070521.
  173. Karimi, N., Zarzbeitia, M., Mariani, A., Gatti, D., Varzi, A., and Passerini, S. (2021). Nonfluorinated ionic liquid electrolytes for lithium metal batteries: ionic conduction, electrochemistry, and interphase formation. *Adv. Energy Mater.* 11, 2003521.
  174. Yoon, H., Lane, G.H., Shekibi, Y., Howlett, P.C., Forsyth, M., Best, A.S., and MacFarlane, D.R. (2013). Lithium electrochemistry and cycling behaviour of ionic liquids using cyano based anions. *Energy Environ. Sci.* 6, 979–986.
  175. Ahmed, F., Choi, I., Ryu, T., Yoon, S., Rahman, M.M., Zhang, W., Jang, H., and Kim, W. (2020). Highly conductive divalent fluorosulfonyl imide based electrolytes improving Li-ion battery performance: additive potentiating electrolytes action. *J. Power Sources* 455, 227980.
  176. Ahmed, F., Rahman, M.M., Chandra Sutradhar, S., Lopa, N.S., Ryu, T., Yoon, S., Choi, I., Lee, S., and Kim, W. (2019). Novel divalent organo-lithium salts with high electrochemical and thermal stability for aqueous rechargeable Li-ion batteries. *Electrochim. Acta* 298, 709–716.
  177. Sasaki, Y. (2008). Organic electrolytes of secondary lithium batteries. *Electrochemistry* 76, 2–15.
  178. von Aspern, N., Röschenthaler, G.V., Winter, M., and Cekic-Laskovic, I. (2019). Fluorine and lithium: ideal partners for high-performance rechargeable battery electrolytes. *Angew. Chem. Int. Ed. Engl.* 58, 15978–16000.
  179. Li, T., Zhang, X.-Q., Shi, P., and Zhang, Q. (2019). Fluorinated solid-electrolyte interphase in high-voltage lithium metal batteries. *Joule* 3, 2647–2661.
  180. Chen, L., Fan, X., Hu, E., Ji, X., Chen, J., Hou, S., Deng, T., Li, J., Su, D., Yang, X., et al. (2019). Achieving high energy density through increasing the output voltage: a highly reversible 5.3 V battery. *Chem* 5, 896–912.
  181. Markevich, E., Salitra, G., Afri, M., Talyosef, Y., and Aurbach, D. (2020). Improved performance of Li-metal|LiNi 0.8 Co 0.1 Mn 0.1 O 2 cells with high-loading cathodes and small amounts of electrolyte solutions containing fluorinated carbonates at 30 °C–55 °C. *J. Electrochem. Soc.* 167, 070509.
  182. Holoubek, J., Yu, M., Yu, S., Li, M., Wu, Z., Xia, D., Bhaladhare, P., Gonzalez, M.S., Pascal, T.A., Liu, P., and Chen, Z. (2020). An all-fluorinated ester electrolyte for stable high-voltage Li metal batteries capable of ultra-low-temperature operation. *ACS Energy Lett.* 5, 1438–1447.
  183. Wang, Q., Yao, Z., Zhao, C., Verhallen, T., Tabor, D.P., Liu, M., Ooms, F., Kang, F., Aspuru-Guzik, A., Hu, Y.-S., et al. (2020). Interface chemistry of an amide electrolyte for highly reversible lithium metal batteries. *Nat. Commun.* 11, 4188.
  184. Sasaki, Y., Shimazaki, G., Nanbu, N., Takehara, M., and Ue, M. (2019). Physical and electrolytic properties of partially fluorinated organic solvents and its application to secondary lithium batteries: partially fluorinated Dialkoxyethanes. *ECS Trans* 16, 23–31.
  185. Ma, P., Mirmira, P., and Amanchukwu, C.V. (2021). Effect of building block connectivity and ion solvation on electrochemical stability and ionic conductivity in novel fluoroether electrolytes. *ACS Cent. Sci.* 7, 1232–1244.
  186. Shiga, T., Kato, Y., Kondo, H., and Okuda, C. (2017). Self-extinguishing electrolytes using fluorinated alkyl phosphates for lithium batteries. *J. Mater. Chem. A* 5, 5156–5162.
  187. Su, C.C., He, M., Peebles, C., Zeng, L., Tornheim, A., Liao, C., Zhang, L., Wang, J., Wang, Y., and Zhang, Z. (2017). Functionality selection principle for high voltage lithium-ion battery electrolyte additives. *ACS Appl. Mater. Interfaces* 9, 30686–30695.
  188. Zheng, Q., Yamada, Y., Shang, R., Ko, S., Lee, Y.-Y., Kim, K., Nakamura, E., and Yamada, A. (2020). A cyclic phosphate-based battery

- electrolyte for high voltage and safe operation. *Nat. Energy* 5, 291–298.
189. Yue, Z., Mei, X., Dunya, H., Ma, Q., McGarry, C., and Mandal, B.K. (2018). Synthesis and physical properties of new fluoroether sulfones. *J. Fluor. Chem.* 216, 118–123.
190. Su, C.-C., He, M., Redfern, P.C., Curtiss, L.A., Shkrob, I.A., and Zhang, Z. (2017). Oxidatively stable fluorinated sulfone electrolytes for high voltage high energy lithium-ion batteries. *Energy Environ. Sci.* 10, 900–904.
191. Jiang, Z., Zeng, Z., Liang, X., Yang, L., Hu, W., Zhang, C., Han, Z., Feng, J., and Xie, J. (2021). Fluorobenzene, a low-density, economical, and bifunctional hydrocarbon cosolvent for practical lithium metal batteries. *Adv. Funct. Mater.* 31, 2005991.
192. Yoo, D.-J., Yang, S., Kim, K.J., and Choi, J.W. (2020). Fluorinated aromatic diluent for high-performance lithium metal batteries. *Angew. Chem. Int. Ed. Engl.* 59, 14869–14876.
193. Mei, X., Yue, Z., Tufts, J., Dunya, H., and Mandal, B.K. (2018). Synthesis of new fluorine-containing room temperature ionic liquids and their physical and electrochemical properties. *J. Fluor. Chem.* 212, 26–37.
194. Hernández, G., Naylor, A.J., Chien, Y.C., Brandell, D., Mindemark, J., and Edström, K. (2020). Elimination of fluorination: the influence of fluorine-free electrolytes on the performance of LiNi<sub>1</sub>/3Mn<sub>1</sub>/3Co<sub>1</sub>/3O<sub>2</sub>/Silicon–Graphite Li-ion battery cells. *ACS Sustain. Chem. Eng.* 8, 10041–10052.
195. Pham, T.D., and Lee, K.-K. (2021). Simultaneous stabilization of the solid/cathode electrolyte interface in lithium metal batteries by a new weakly solvating electrolyte. *Small* 17, e2100133.
196. Holoubek, J., Liu, H., Wu, Z., Yin, Y., Xing, X., Cai, G., Yu, S., Zhou, H., Pascal, T.A., Chen, Z., and Liu, P. (2021). Tailoring electrolyte solvation for Li metal batteries cycled at ultra-low temperature. *Nat. Energy* 2021, 303–313.
197. Logan, E.R., and Dahn, J.R. (2020). Electrolyte design for fast-charging Li-ion batteries. *J. Trends Chem.* 2, 354–366.
198. Qi, S., He, J., Liu, J., Wang, H., Wu, M., Li, F., Wu, D., Li, X., and Ma, J. (2021). Phosphonium bromides regulating solid electrolyte interphase components and optimizing solvation sheath structure for suppressing lithium dendrite growth. *Adv. Funct. Mater.* 31, 2009013.
199. Schmuck, R., Wagner, R., Hörpel, G., Placke, T., and Winter, M. (2018). Performance and cost of materials for lithium-based rechargeable automotive batteries. *Nat. Energy* 3, 267–278.
200. Jaumaux, P., Wu, J., Shanmukaraj, D., Wang, Y., Zhou, D., Sun, B., Kang, F., Li, B., Armand, M., and Wang, G. (2021). Non-flammable liquid and quasi-solid electrolytes toward highly-safe alkali metal-based batteries. *Adv. Funct. Mater.* 31, 2008644.
201. Hou, J., Lu, L., Wang, L., Ohma, A., Ren, D., Feng, X., Li, Y., Li, Y., Ootani, I., Han, X., et al. (2020). Thermal runaway of lithium-ion batteries employing LiN(SO<sub>2</sub>F)<sub>2</sub>-based concentrated electrolytes. *Nat. Commun.* 11, 5100.
202. Boyle, D.T., Huang, W., Wang, H., Li, Y., Chen, H., Yu, Z., Zhang, W., Bao, Z., and Cui, Y. (2021). Corrosion of lithium metal anodes during calendar ageing and its microscopic origins. *Nat. Energy* 6, 487–494.
203. Wood, S.M., Fang, C., Dufek, E.J., Nagpure, S.C., Sazhin, S.V., Liaw, B., and Meng, Y.S. (2018). Predicting calendar aging in lithium metal secondary batteries: the impacts of solid electrolyte interphase composition and stability. *Adv. Energy Mater.* 8, 1801427.
204. Xia, J., Madec, L., Ma, L., Ellis, L.D., Qiu, W., Nelson, K.J., Lu, Z., and Dahn, J.R. (2015). Study of triallyl phosphate as an electrolyte additive for high voltage lithium-ion cells. *J. Power Sources* 295, 203–211.
205. Lee, Y.M., Seo, J.E., Lee, Y.-G., Lee, S.H., Cho, K.Y., and Park, J.-K. (2007). Effects of Triacetoxymethylsilane as SEI layer additive on electrochemical performance of lithium metal secondary battery. *Electrochim. Solid-State Lett.* 10, A216.
206. Sun, Y.-K. (2021). An experimental checklist for reporting battery performances. *ACS Energy Lett.* 6, 2187–2189.
207. Stephan, A.K. (2021). Standardized battery reporting guidelines. *Joule* 5, 1–2.
208. Adams, B.D., Zheng, J., Ren, X., Xu, W., and Zhang, J.-G. (2018). Accurate determination of coulombic efficiency for lithium metal anodes and lithium metal batteries. *Adv. Energy Mater.* 8, 1702097.